QATAR UNIVERSITY

COLLEGE OF HEALTH SCIENCES

DEVELOPMENT AND IN VIVO TESTING OF SMART NANOPARTICLES FOR ENHANCED ANTI-CANCER ACTIVITY AND REDUCED CARDIOTOXICITY ASSOCIATED WITH TYROSINE KINASE INHIBITORS

BY

HISSA FALEH AL-THANI

A Thesis Submitted to

the College of Health Sciences

in Partial Fulfillment of the Requirements for the Degree of

Masters of Science in Biomedical Sciences

June 2021

COMMITTEE PAGE

The members of the Committee approve the Thesis of
Hissa Al-Thani defended on [Defense Date].

Dr. Huseyin C. Yalcin
Thesis/Dissertation Supervisor

Dr. Katerina Gorachinova
Committee Member

Dr. Hesham Korashy
Committee Member

Dr. Layla Kamareddine
Committee Member

Dr. Shahab Uddin
Committee Member

.

Approved:

Hanan Abdul Rahim, Dean, College of Health Science

ABSTRACT

AL-THANI, HISSA, F., Masters of Science: June : [2021:], Biomedical Sciences

Title: Development and in Vivo Testing of Smart Nanoparticles for Enhanced Anti-Cancer Activity and Reduced Cardiotoxicity Associated with Tyrosine Kinase Inhibitors

Supervisor of Thesis: Dr. Huseyin C. Yalcin.

Tyrosine kinase inhibitors (TKIs) are new generation of anti-cancer drugs with very high efficiency against cancer cells. However, TKIs are associated with severe cardiotoxicity limiting their clinical benefits. One particular TKI that has been developed recently but not explored much is Ponatinib. The use of nanoparticles as a better therapeutic agent to deliver anti-cancer drugs and reduce their cardiotoxicity has been recently considered. In this study, PLGA-PEG-PLGA nanoparticles were synthesized to deliver Ponatinib while reducing its cardiotoxicity for treatment of chronic myeloid leukemia. Shape, size, surface charge and drug uptake ability of these nanoparticles were assessed using transmission electron microscopy (TEM), ZetaSIZER NANO and high-performance liquid chromatography (HPLC). Cardiotoxicity of Ponatinib, unloaded and loaded PLGA-PEG-PLGA nanoparticles were studied on zebrafish model through measuring the survival rate and cardiac function parameters, to optimize efficient drug concentrations in an in vivo setting. These particles were tested on zebrafish cancer xenograft model in which, K562 cell line, was transplanted into zebrafish embryos. We showed that, at an optimal concentration (0.0025mg/ml), Ponatinib loaded PLGA-PEG-PLGA particles are non-toxic/non-cardio-toxic and are very efficient against cancer growth and metastasis.

DEDICATION

To all those people out there fighting cancer

ACKNOWLEDGMENTS

First and foremost, I would like to express my sincere gratitude to the Biomedical Research Center (BRC) for giving me the opportunity to conduct my thesis research. I would like to thank my supervisor Dr. Huseyin C. Yalcin for his for his continuous guidance, support and patience.

Secondly, I would like to thank the Center for Advanced Materials (CAM) and the Central Laboratories Unit (CLU) lab members for their assistance in performing some of the data analysis. And I extend my heartfelt thanks to Dr. Zain Zakaria, Ms. Samar Shurbaji, a research assistance at BRC and Ms. Hadeel Al-Jighefee, a graduate research assistant at the BRC for their ongoing assistance, support and always being at my side.

Last and certainly not least, I would like to express my special thanks to my family and friends for their unconditional support, well wishes and the continues encouragements that helped me in putting forth my best in this project.

TABLE OF CONTENTS

LIST OF TABLES

LIST OF FIGURES

Chapter 1: Introduction

1.1 Introduction

Cancer is the second leading cause of death worldwide with high number of incidents [1]. Cancer arises from mutations that cause activation of oncogenes or/and inactivation of the tumor suppressor genes leading to uncontrolled cell growth and proliferation, which further trigger other complications in the body that eventually might lead to death [2]. Leukemia is a type of cancer that is characterized by the uncontrolled growth of the hematopoietic stem cells from the bone marrow [3]. There are several subtypes of leukemia and the most encountered subtype among adults is the Chronic Myeloid leukemia (CML) [3]. CML is generally diagnosed by the presence of the Philadelphia chromosome that harbor the *BCR-ABL* oncogene, which would cause abnormal cell proliferation and complications in the patients [4].

Therefore, the demand for successful anti-cancer therapeutics and developing of effective tools for early cancer detection and screening have been increased. For example, the evolving of the Tyrosine Kinase inhibitors (TKIs) [5] such as, Imatinib, Nilotinib, Ponatinib and Dasatinib as anti-cancer drugs particularly for CML had aid in improving the overall outcomes of the patients and increasing their survival rates [6]. However, due to some encountered toxicity of these drugs especially in the heart [7], the usage of nanotechnology to treat the cancer has been raised. This is because nanoparticles (NPs) are known to be more effective and precise in targeting cancer cells and reduce toxicity associated with the anti-cancer drugs [8].

zebrafish have been used as a research model in many applications such as, in cancer studies due to their numerous advantages. For example, they have high genetic resemblance to humans with about 70% orthologue genes, making it a useful model for genetic manipulation [9]. Moreover, they are easy to maintain, have short maturation and developing time and the transparent embryos have made imaging and studying the internal organs such as the heart

much easier [10]. In addition, due to their lack of adaptive immunity during the first months of development, zebrafish is a good model for xenotransplantation of human tumor cells in order to develop a cancer model to study human cancers and testing of the anti-cancer drugs [11].

1.2 Hypothesis:

Delivery of Ponatinib, a TKI drug, using smart NPs into CML cells increases the anti-cancer activity and reduces cardiotoxicity in the zebrafish xenograft model in comparing with the use of TKIs drugs alone.

1.3 Objectives:

- To produce smart nanoparticles (PLGA-PEG-PLGA) and define their characteristics.
- To generate a zebrafish xenograft model of CML cancer.
- To test for the toxicity of TKIs and the generated NPs on normal zebrafish.
- To determine the efficacy of the generated NPs as effective anti-cancer drug delivery system by testing them on the zebrafish xenograft model.

Chapter 2: Literature Review

2.1 Cancer

Cancer is the second main cause of death worldwide after the cardiovascular disease [1] with increasing incidences and death rates worldwide throughout the years [12]. Cancer is described as uncontrolled cell growth that gains metastatic properties in response to the activation of oncogenes and/or deactivation of the tumor suppressor genes [2].

2.1.1 Prevalence of cancer

According to the GLOBOCAN (2018), the estimated number of the new cancer cases had reached to 18.1 million and the deaths are about 9.6 million [13] and by the year 2030 it has been estimated that the cancer death count would reach to 30 million per year [14]. Therefore, new tools for early detection and diagnosis of cancer are essential as well as developing effective therapeutic agents for cancer treatment such as, nanotechnology are the key to reduce cancer mortality and incidences [15]. In Qatar, the overall incidence rate in 2014 was 66.02 per 100,000 and the most common cancers among the population were beast, colorectal and prostate cancers and the burden of cancer is estimated to increase more by 2030 [16]. Leukemia is also one of the major cancers in Qatar with an incidence of 8.5 per 100,000 and 4.8 per 100,00 for males and females, respectively [17].

2.1.2 Chronic Myeloid Leukemia

Leukemia is a common malignancy in pediatrics and adults that arises from alternations in cell regulatory processes to cause unregulated proliferation of the hematopoietic stem cells of the bone marrow leading to the development of different subtypes of leukemia with different characteristics such as acute myelogenous, chronic myelogenous, acute lymphoblastic and chronic lymphoblastic leukemia and the most common leukemia that almost exclusively occurs in adults is the chronic myeloid leukemia [3]. Chronic myeloid leukemia (CML) is a myeloproliferative neoplasm that is characterized by the excessive number of granulocytes,

which are neutrophils, eosinophils and basophils and it is also known as a clonal disorder of the hematopoietic stem cells of the bone marrow [4]. The incidence of CML is 1-2 cases per 100,000 adults and about 15% of the newly diagnosed cases of leukemia in adults accounts for CML [18]. CML is diagnosed genetically by the presence of the abnormal chromosome, the Philadelphia chromosome [4]. Philadelphia chromosome is formed by the oncogene BCR-ABL fusion, in which the 3' portion of the Abelson (ABL) gene on the long arm of chromosome 9 is combined with the 5' portion of the breakpoint cluster region (BCR) gene located on the long arm of chromosome 22 [4]. The BCR-ABL fusion oncogene is associated with irregular proliferation of the myeloid cells, cytogenetic abnormalities as the disease proliferate and treatment resistance in case of mutations in the BCR-ABL kinase domain [4]. As, the constitutively active tyrosine kinase BCR-ABL would promote growth and proliferation by the downstream signaling pathways such as, JUN kinase, STAT and RAS [19-21]. There are three phases of CML, chronic, accelerated and blast phases [4].

2.2 Smart Nanoparticles

Nanoparticles (NPs) are small particles with a size range from 1 to 1000 nm [22] that can be engineered to gain unique compositions and functions in order to be used as tools in research areas [23]. NPs come in several types of different sizes, structures and functions, which can then be classified accordingly. For instance, they can be categorized based on their material type into: 1. carbon-based nanoparticles, in which the particles contain carbon such as, graphene (Gr) and carbon black [24]; 2. Inorganic-based nanoparticles, the particles made of metals (Au or AG) or metal oxides (TiO2 or ZnO) or from semiconductors (Ceramics or Silicon); 3. Organic-based nanoparticles, where the particles are from organic materials that transformed into unique structures such as, liposomes, micelles and polymers; 4. Composite-based nanoparticles are NPs that combine multiple other NPs or materials [25].

2.2.1 Applications of Nanoparticles

NPs have been utilized in many research and biomedical purposes due to their several advantages. To illustrate this, NPs can be used as sensors and pathogen detector, using surface ligands to amplify the detection and specific binding of the analytes [23] and the most used type of NP biosensors are the inorganic NPs, particularly the metallic or magnetic NPs [26]. Also, NPs are used to detect pathogens as bacteria throughout magnetic NPs that are coated with antibodies against the bacterial surface antigens [27]. NPs also work as sensitive tools for specific cell detection and separation [23]. For example, circulating tumor cells (CTCs), act as biomarkers to determine the prognosis and overall survival levels in metastatic colorectal, prostate and breast cancers' patients [28, 29], are identified and captured through the NP immunomagnetic technique [30]. In addition, NPs are promising tools to attribute in targeted imagining, because of their surface area they could deliver large number of imaging agents at a time, thus enhancing the sensitivity [31]. Lastly, the NPs can also work as delivery vehicles to facilitate the entry of some agents into the cells such as, the entrance of the Small interfering RNA (siRNA) into the cells allowing it to splice and degrade the mRNA for gene function studies [32]. NPs as delivery vehicles can also aid in carrying agents such as drugs to treat various diseases for example, diabetes, neurological disorders and cancer [33]; this is due to their ability to protect the load from getting degraded and in controlling the drug release by improving drug's accumulation in diseased tissue and decreasing its clearance, therefore the therapeutic efficacy would increase and drug side effects would be reduced [34].

2.2.2 Nanoparticles in cancer

Over the past several decades, nanotechnology has made critical contribution in cancer studies [35] as it helped in early diagnosis of several cancers such as breast and colorectal cancers, through enhancing the imaging and screening techniques and hence improving the outcomes of the patients [36]. Moreover, NPs are also applied as effective therapeutic agents for cancer treatments due to their ability of targeted delivery, drug storage, tumor imaging and

overcoming resistibility, solubility and stability problems [8]. The first type of therapeutic NPs to receive clinical approval for cancer treatment is the Liposomes [37] e.g. Daunoxome and Doxil that are effective in treating breast and ovarian cancers [38].

2.2.3 Toxicity of Nanoparticles

The toxicity of the nanomaterials could be seen at different levels i.e., on the molecular, cellular as well as on the tissue level [34]. This is due to the ability of those particles to move easily through the body, and getting exposed to several biological microenvironments such as, the body fluids (e.g., blood), the extracellular matrix, the cytoplasm and to the cell organelles [34].

To illustrate that, the iron oxide nanoparticles have been reported to cause effects on the molecular level by irreversibly changing the structure and function of the transferrin protein upon its binding to the particles leading to a permanently damage in the iron transport [39]. Also, NPs have been shown to affect the folding ability of fibrinogen that stimulates the inflammatory signaling pathways [40].

The cellular toxicity of the NPs could be illustrated by the ability of some NPs such as, zinc oxide [41], polycation particles [42], titanium oxide [43] and polystyrene nanoparticles [44] to disrupt the cell lysosome membrane. Consequently, this would cause the release of iron, protons and hydrolytic enzymes that results in protein aggregation, oxidative stress, mitochondrial dysfunction and endoplasmic reticulum (ER) stress [45].

Moreover, NPs have the ability to cause toxicity on the tissue level especially on the organs with the highest NP accumulation level such as the liver after intravenous injection and the lung after intratracheal installation [34]. For example, hepatotoxicity has been reported by the presence of high levels of the liver enzymes in the blood after administrating positively charged lipid nanoparticles [46].

Exposure to nanoparticles have also studied to cause cardiac toxicity and subsequently

myocardial damage as a result of increased production of reactive oxygen species (ROS) and redox homeostasis alternation [47]. For instance, following to the exposure of titanium dioxide (TiO2) NPs has showed to increase ROS levels, reduced malondialdehyde and increased the DNA peroxidation in the cardiac muscles. While long exposure to TiO2 NPs has resulted into sparse cardiac muscle fibers, cardiac biochemical derangement, tissue inflammatory response and cell necrosis [48]. Moreover, toxicities associated with zinc oxide (ZnO) NPs have also been reported after testing these NPs on a rat animal model [49]. The toxicity was seen as an inflammation in the lung tissues and a myocardial damage after exposing the rats for a long period of time to ZnO NPs [49]. Also, oral administration of ZnO NPs by the rats showed to cause inflammation, DNA damage and apoptosis in the rats' hearts as well as for the high levels of cardiac biomarkers such as troponin T, CPK-MB and myoglobin, that have been detected in the rats [50].

2.3 Tyrosine Kinase

Tyrosine kinase protein is an enzyme that catalyzes the process of transferring the gamma – phosphate group from an ATP molecule to tyrosine residues of numerous essential proteins, causing protein phosphorylation and signal transferring that aid in regulating cell cycle, cell proliferation, death and other several biochemical and physiological mechanisms [30].

2.3.1 Tyrosine Kinase types

The tyrosine kinases are divided into two types according to their structure: Receptor tyrosine kinases (RTK) and Non-receptor (NRTKs) or cellular tyrosine kinases. RTK is located on the cell surface and have an extracellular ligand binding domain, a transmembrane domain and an intracellular kinase domain [51]. RTKs would bind to ligands and cause phosphorylation of the tyrosine residues of the target proteins and then transmit signals through the signaling transduction pathways such as, RAS/RAF/MEK/ERK and PI3K/AKT/mTOR to

activate biochemical cascades within the cells [52] while the NRTKs are located either in the cytoplasm or in the nucleus that aid in the downstream signal transduction cascades. [53].

2.3.2 Tyrosine Kinases in Cancer

Disorders of tyrosine kinase proteins could lead to the development of serious diseases in the body, as mutations in these proteins are overrepresented by about four-fold compared with a random selection of genes and they are the most family of genes contribute to neoplastic disorders when they are mutated [54, 55]. It has been determined that tyrosine kinase proteins in healthy cells act as tumor suppressors or proto-oncogenes. However, aberrations in these proteins could cause irregular cell proliferation and eventually tumorigenesis, as more than 50% of the proto-oncogenes and oncogenes expressing abnormal tyrosine kinase would be activated [56]. Moreover, tumor invasion, metastasis, angiogenesis and chemotherapy resistance are also seen due to the abnormal expression of tyrosine kinase protein [57].

For example, mutations within the extracellular domain such as the EGFRv III mutation would cause a constitutive activity of the tyrosine kinase receptor that eventually leads to uncontrolled cell proliferation and this mutation have been seen in non-small cell lung carcinoma, glioblastomas and ovarian tumors [58, 59]. Also, cervical and human bladder carcinomas have been associated with somatic mutations in EGFR 2 and EGFR 3 [59]. The BCR-ABL chimeric gene responsible for CML development has higher tyrosine kinase activity by several folds than its normal equivalent that relates to the disease phenotype [60].

2.4 Tyrosine Kinase Inhibitors

Due to the involvement of tyrosine kinases in cancer, international research institutions and pharmaceutical groups have determined tyrosine kinase proteins as targets for anti-cancer drug research, such as the development of tyrosine kinase inhibitors (TKI) [5]. TKIs are designed to block aberrant signals of the signaling transduction pathways that are associated to cell growth and proliferation and they are developed to either inhibit one or two tyrosine

kinases or even more tyrosine kinases in multiple signaling pathways. To do that, the TKIs would compete with the ATP for the ATP binding site of the tyrosine kinase and thus reducing the phosphorylation of the tyrosine kinase residues [61]. Consequently, this would assist in the anti-cancer mechanism of TKIs by causing tumor cell arrest in G1 phase, inhibition of tumor cells' repair, induction of anti-angiogenesis and apoptosis. Also, these TKIs can be divided according to their main targets, VEGFR inhibitors, Bcr-Abl inhibitors, EGFR inhibitors and anaplastic lymphoma kinase (ALK) inhibitors [62, 63].

2.4.1 Tyrosine Kinase Inhibitors as anti-cancer agents

One example of a cancer that have been treated with TKIs is the Chronic Myeloid Leukemia (CML), as the outcomes of patients with CML have been transformed over the past fifteen years due to TKI therapy [64]. TKIs block the proliferation of the malignant cells by interfering with the BCR-ABL oncoprotein and adenosine triphosphate interaction [64]. Currently, for the first-line treatment of the CML chronic phase, the Food and Drug Administration (FDA) had approved three TKIs: Imatinib, Nilotinib and Dasatinib. Imatinib showed to be better than combination of interferon and cytarabine therapy, in terms of tolerability, cryptogenic and hematologic responses as well as in reducing the chances of developing the accelerated- or blast- phases of CML [6]. However, patients who are first-line TKI therapy intolerant or noncompliant, would have the second-line TKI therapy that include the second generation of TKIs, Nilotinib, Dasatinib and Bosutinib [64]. Although the third generation TKI, Ponatinib was the third-line treatment of choice, it has been seen to be associated with high risk of developing arterial and venous thromboembolism. Thus, only patients with the threonine-to-isoleucine mutation at position 315 (T315I), would have it as its more effective in those patients [65].

2.4.2 Toxicity of Tyrosine Kinase Inhibitors

Toxicity profiles of each TKI drug should be determined before usage, as TKIs could

cause toxicity when they are taken alone or in combination. And their toxicity is either linked to their main target kinase, off-target consequence or due to a specific kinase inhibitor metabolite [66]. The most common side effects of TKIs are rash and diarrhea [67]. However, there are other side effects of the drugs that are explained by their action on normal tissues such as on the liver, heart and eyes [68, 69].

The most concern of TKIs side effects is the cardiotoxicity in the cancer patients treated with those drugs [70]. For instance, several patients who have took Imatinib as an anti-cancer drug have expressed left ventricular dysfunction [71]. Also, compromised hemodynamics, pulmonary hypertension and cardiac failure have been observed as cardiotoxicity effects of the Dasatinib drug [72]. Ponatinib, a TKIs drug, have also showed adverse effects on the cardiovascular such as, heart failure, arterial occlusive events and hypertension [73].

2.5 Zebrafish Model

Nowadays, zebrafish are being used as a model in different studies such as, in behavioral, developmental, physiological, immunity and genetic studies [10]. Zebrafish or Danio rerio, in Latin, are small fish of the tropical freshwater that originates from the Ganges River [74] and they were first suggested as a research model by George Streisinger and his colleagues at Oregon University [75]. The advantages of using zebrafish as an animal model are, their genome is fully sequenced and easy to be manipulated, they have high fertility rate, rapid embryonic development (within 24 hours), short maturation period (3 months), the embryos' organs and systems such as, the heart, the blood vessels and the intestine would be completed after 48 hours post-fertilization and the translucent embryos would aid in studying the embryogenesis developmental stages [10]. Moreover, there are several zebrafish transgenic lines and more than ten thousand mutants in the fish protein coding genes have been generated to help in studying human diseases, such as cardiovascular diseases, neural disorders and cancer [9]. In addition, the zebrafish genome has a high genetic similarity with the human

genome, as it has been estimated that at least 70% of the human genes have orthologue genes in the zebrafish genome [9]. Although, there are several strains of zebrafish worldwide, the only strains that are usually used in research laboratories are, AB, EKKwill, Casper, Tubingen, Nadia, wild-caught and Wild India Karyotype [10].

2.5.1 Zebrafish Xenograft model

Zebrafish are also being used as a model for the human cancers to test for the chemicals and drugs carcinogenicity and toxicity [76]. They spontaneously respond to carcinogens [77, 78] and mutagens [79] and thus develop malignant tumors [79], with a tendency to increase in unstable genetic background or in loss of tumor suppressor functions such as, p53 [80]. Moreover, transgenesis of several types of common human tumors have been exhibited in zebrafish, for example, lung cancer, breast cancer, ovarian carcinoma, prostate cancer, leukemia and retinoblastoma [81]. This transplantation of human cancer cells into zebrafish, endorsed that the molecular mechanisms of mammalian tumorigenesis is similar in zebrafish [82]. Moreover, the transplantation of the cancer cells is possible due to the lack of an adaptive immune system during the first months of developing [83].

Chapter 3: Materials and Methods

3.1 List of Materials

- RPMI Medium 1640 (1X) (Gibco® Laboratories, Thermo Fisher Scientific, USA)
- Human CML K-562 cell lines (ATCC® CCL-243™)
- Recovery™ Cell Culture Freezing Medium (Gibco® Laboratories, Thermo Fisher Scientific, USA)
- FBS, Qualified, HI (Gibco® Laboratories, Thermo Fisher Scientific, USA)
- DMSO (Dimethyl sulfoxide), anhydrous (Invitrogen™, Thermo Fisher Scientific, USA)
- CellTracker™ CM-Dil (Invitrogen™, Thermo Fisher Scientific, USA)
- Penicillin-Streptomycin Antibiotic (Gibco® Laboratories, Thermo Fisher Scientific, USA)
- Pluronic F-127 (Sigma Aldrich, Germany)
- DPBS (1X) (Gibco® Laboratories, Thermo Fisher Scientific, USA)
- Poly(lactide-co-glycolide)-fluorescein (Sigma Aldrich, Germany)
- PLGA-PEG-PLGA (MW: 6000:10,000:6000 Da) (Akina, Inc., USA)
- Ponatinib Free Base (LC Labs, USA)
- PBS pH 7.4 (1X) (Gibco® Laboratories, Thermo Fisher Scientific, USA)
- Tricaine
- Tetrahydrofuran (VWR International, USA)
- Milli Q Water purified by Milli Q system (Millipore, Molsheim, France)
- Pronase
- Egg Water
- 1-phenyl 2-thiourea (PTU)
- Trypan Blue Solution, 0.4% (Gibco® Laboratories, Thermo Fisher Scientific, USA)

- GlutaMAX (Gibco® Laboratories, Thermo Fisher Scientific, USA)

3.2 List of Equipment

- KOVA™ Glasstic™ Slide 10 with Grids (Fisher Scientific, USA)
- Confocal Microscopy
- Transmission electron microscope (TEM)
- Olympus fluorescent microscopy
- Analytical balance
- Zebrafish imaging concave slide
- Syringe Filter 0.45µm
- Syringe Filter 0.2µm
- Spectra-Por® Float-A-Lyzer® G2 membrane
- Cryogenic Tubes
- Vivaspin® 20 Ultrafiltration Unit (Sartorius Stedim Biotech, Germany)

3.3 Methods

3.3.1 Cell culture:

Human CML K-562 cell line was obtained from ATCC and from the Interim Translational Research Institute (iTRI) at Hamad Medical Corporation (HMC). Cells have been cultured according to the optimum conditions described by the manufacturer. The cells have been cultured in RPMI 1640 (Gibco) supplemented with 10% FBS (Gibco), 10,000 U/mL Penicillin-Streptomycin (Gibco) and 100X GlutaMAX (Gibco) at 37°C in a humidified 5% CO2 incubator. The cells' media were changed every alternative day to obtain the optimum cell count and maintain their viability at 90% following this equation: No. of viable cells / total No. of cells x 100. The cell counting was performed by taking out all the solution from the T75 flasks into falcon tubes (15ml or 50ml), centrifuged at 1300 rpm for 5 min, the supernatant is discarded and then the pellets are re-suspended in 3-2 ml RPMI 1640 (Gibco) media. Then the

cell count was done manually using a KOVA™ Glasstic™ Slide 10 with Grids (Fisher Scientific) by taking 20µL of the cell suspension mixed with 20µL of the trypan blue stain and then 20µl of the mixture was loaded in the hemocytometer. Only the cells in the large 4 squares at the edges were counted under a light microscope. After that, the cell count in a ml was done following the equation: cell count x dilution factor (2) x the hemocytometer constant (10^4). After that to determine how much media were required to add into each T-75 flask for passaging the cells the following equation have been followed:

$$\frac{\text{No. of cell count x how much media was added to the pellet x 2}}{8\text{x}10^5}$$

3.3.2 Fluorescent labeling of CML cells prior to xenotransplantation:

Once the K-562 cells have reached confluency (1 x 10^6 cells/mL), they have been harvested by pelleting using a centrifuge at 1200 rpm for 5 minutes, the supernatant is then discarded then re-suspended in 3ml PBS mixed with 6µl 5 µg/ml CM-Dil fluorescent dye (Invitrogen). Then the dyed cells were incubated for 5 min at 37 °C followed by a 15 -20 min incubation at 4°C. After that, the cells were checked under the fluorescence microscope using fluorescent filters with excitation/emission spectra of 553/570 nm maxima.

3.3.3 Tyrosine Kinase Inhibitor (TKI) Exposure Toxicity:

The toxicity of the TKI drugs (i.e Ponatinib) was determined with the aid of Dr. Huseyin C. Yalcin lab member, Dr. Zain, a PhD graduate student. This was done by placing the fertilized embryos at 24 hpf in a 6-well cell culture plates with 20 embryos per well in 3 ml of the solution. Normal group were exposed to embryo media (EM). Negative control group was exposed to EM plus DMSO or PBS as vehicle, since drugs are dissolved in DMSO or PBS as needed to prepare the stock solutions. The experimental group was exposed to working solutions with different concentrations (0, 0.01, 0.1, 1, 10, 25, 50, and 100 mg/L) of the tested TKIs (Ponatinib). Doxorubicin and Imatinib have served as positive controls since these drugs

have known adverse cardiac toxicities. Then the embryos were placed in the incubator at 28°C and at the following days the survival rate was measured, and heart and tail videos were taken at 3dpf.

3.3.4 Zebrafish husbandry:

Wild-type zebrafish embryos (AB strain) were used for this experimentation. All animal experiments were carried out according to national and international guidelines for the use of zebrafish in experimental settings [84] and in accordance with the animal protocol guidelines required by the Qatar University and policy on zebrafish research established by department of research in the Ministry of Public Health, Qatar (Ministry of Public Health, 2017). This study has been approved by the Institutional Animal Care and Use Committee (IACUC); the approval document (QU-IACUC 019/2020) is found in the Appendix section (chapter 6).

3.3.5 Xenografts injection procedure:

The zebrafish embryos were exposed to Pronase at 24 hours post fertilization to remove the chorion. After that they were incubated till 2- or 3-days' post fertilization (dpf) at 28°C. Dechorionated embryos were transferred to an injection slide and they were anesthetized with 1% Tricane solution for destabilization. After that the fluorescently labeled K562 cells were injected to the yolk sac to allow the cells to enter into the blood circulation using a fashioned glass capillary needle. About 300 of the cancer cells' K562 have been injected per embryo, using the Femtojet injector (Eppendorff) at the BRC zebrafish facility. The embryos were first anesthetized with 200mg/L Trican for 5 minutes and were aligned properly to have their body on one site to allow easier access to their yolk sacs. Then a capillary needle that have been prepared using borosilicate glass microcapillaries following the setting: air pressure, 500; heat, 650; pull, 100; velocity, 200; time, 40, was used. A 10µl of the cells' solution were then loaded into the needle and the needle is placed into a manipulator and adjust manipulator until holding

the needle with 45^{o} angle with respect to embryo, the needle tip is break with tweezers and the cells' solution was genteelly injected into the zebrafish embryos' yolk sacs. After that the xenotransplanted embryos were transferred into new plates and fresh egg water and kept at 34 °C till the end point at 7dpf. The zebrafish larvae were imaged under the fluorescence microscope using the ZEISS ZEN Microscope Software each day after injection to check the cancer cell spread and measure the tumor size.

3.3.6 Preparation of the NPs:

The PLGA- PEG- PLGA polymers were used to generate our NPs. 25mg of PLGA- PEG- PLGA polymers (Mw 6000:10000:6000) were measured by the analytical balance and added to a beaker along with 5mg of the fluorescently labeled PLGA with 5DTAF in order to have our particles to be fluorescent and then 10ml of THF were added with the PLGA polymers in one beaker with a magnetic stirrer and this was the "Organic solution". At the same time but in another beaker along with a magnetic stirrer, 5mg Pluronic F127 was added in 20 ml milli Q water and this was the "water solution". After that the organic solution was transferred into the water solution, very slowly, in a drop-by-drop approach to induce nanoprecipitation and embryonic nanoparticles formation. Finally, the dispersion was kept for overnight with a magnetic stirrer to evaporate the organic solvent. In the next day the NPs dispersion was filtered through 0.45 microm filter and the filtrate was placed in the ultrafiltration tube (Vivaspin® 20 Ultrafiltration Unit) (Sartorius Stedim Biotech, Germany) to wash and concentrate the NPs. The tubes were placed in a centrifuge for 10 min 4500 RPM.

3.3.7 TKI loaded NP preparation:

The PLGA- PEG- PLGA polymers were used to generate drug loaded NPs. 25mg of PLGA- PEG- PLGA polymers (Mw 6000:10000:6000) were measured by the analytical balance and added to a beaker along with 5mg of the fluorescently labeled PLGA with 5DTAF in order to have our particles to be fluorescent, and for the TKIs loading, from Ponatinib drug

of 100mM stock concentration a 5mg (100ul), 10mg (200ul) or 15mg (300ul) was added and then 10ml of THF were also added with the PLGA polymers in one beaker with a magnetic stirrer and this was the “Organic solution”. At the same time but in another beaker along with a magnetic stirrer, 5mg Pluronic F127 was added in 20 ml milli Q water and this was the “water solution”. After that the organic solution was transferred into the water solution, very slowly, in a drop-by-drop approach to induce nanoprecipitation and embryonic nanoparticles formation. Finally, the dispersion was kept for overnight with a magnetic stirrer to evaporate the organic solvent. In the next day the NPs dispersion was filtered through 0.45 microm filter and the filtrate was placed in the ultrafiltration tube to wash and concentrate the NPs. The tubes were placed in a centrifuge for 10 min 4500 RPM. After three washing cycles for the free unencapsulated drug and the excess of the surface agent removal. NPs dispersions of a known concentration were prepared by redispersion of the concentrated NPs in a known volume of a milli Q water.

3.3.8 NPs characterization

3.3.8.1 Transmission Electron Microscope (TEM)

TEM, which is a powerful instrument to characterize and image materials such as nanoparticles. TEM has been used to characterize the PLGA-PEG-PLGA nanoparticles. The procedure was carried by the Central Laboratories Unit (CLU) at Qatar University.

3.3.8.2 Scanning Electron Microscope (SEM)

The particles surface morphology was assessed using NOVA NANOSEM 450 (N-SEM) by the Central Laboratories Unit (CLU) at Qatar University. SEM uses a field emission gun as a source of electrons. The electron beam then travels through the column while being adjusted by different lenses till reaching the sample. The electrons interact with the sample producing secondary electrons and characteristic X-rays that can be detected by special detector to produce electron image and elemental spectra correspondingly.

3.3.8.3 Nanoparticles size

Size of PLGA-PEG-PLGA nanoparticles have been measured by Nanosizer 2000 - Malvern. The cuvette was filled by the NPs solution and inserted into the machine after selecting the corresponding refractive index of the NP.

3.3.8.4 Zeta potential measurement

The surface charges of the loaded and unloaded PLGA-PEG-PLGA nanoparticles were determined by the ZetaSIZER NANO -Malvern hosted at the Center for Advanced Materials (CAM) at Qatar University. The machine measures the Zeta potential by using electrophoretic light scattering. The PLGA-PEG-PLGA refractive index was obtained from the literature [85] and the NPs solution was then placed in a disposable folded capillary cell to be processed by the machine.

3.3.8.5 Ponatinib Dissolution Rate

To determine the dissolution rate of the loaded drug in the NPs, a dialysis membrane method have been done. This was performed using the Float-A-Lyzer G2 membrane, which trap the particles inside and allow the loaded drug to be released into the surrounding media. The NPs solution of 1 or 0.5ml have been loaded inside the membrane and the membrane was then placed inside a beaker filled with PBS buffer pH 7.4 with a magnetic stirrer at 37°C for 24hr. After that, samples were taken for analysis from the same spot of the PBS buffer at regular intervals (1hr, 3hr, 5hr and 24hr).

3.3.8.6 High-performance liquid chromatography (HPLC)

HPLC is a technique to identify and quantify components in a mixture. Thus, HPLC analysis have been performed for the dissolution rate samples to identify and determine the presence of Ponatinib drug. This method has been done by the Central Laboratories Unit (CLU) at Qatar University. The eluents were, A) KH2PO4 0.0037 Molar (40%), PH 3.5 by H3PO4. Eluent: B) CH3CN (Acetonitrile) (60%). The flow rate was 1.2 ml/min, and the injection

amount was 5µl. The detector (PDA/UV) at 25nm wavelength and for the standard injected was a 5µl of the standard Ponatinib drug + 200µl of CH3CN (Acetonitrile).

3.3.9 Unloaded NPs Toxicity

The zebrafish embryos at 24 hours post fertilization (hpf) were exposed to 200µl Pronase solution for 10 min to remove the chorion. Dechorionized embryos were then evaluated under the stereo microscope and segregated into 6-wells plate equally (about 20 or 24 embryos in each well). After that different concentrations of the unloaded NPs were prepared to determine the optimum concentration that will not cause any toxicity to the zebrafish embryos. The concentrations that have been prepared by diluting the proper amount of the NPs in PTU are: 1, 0.75, 0.5, 0.25, 0.1mg/ml. After that the PTU solution in the wells was removed and replaced with the diluted NPs solution. The embryos were then incubated at 30°C and survival rate was then measured at 48 hpf and 72 hpf.

3.3.10 Loaded NPs Toxicity

The zebrafish embryos at 24 hours post fertilization (hpf) were exposed to 200µl Pronase solution for 10 min to remove the chorion. Dechorionized embryos were then evaluated under the stereo microscope and segregated into 6-wells plate equally (about 20 or 24 embryos in each well). After that different concentrations of the three groups of loaded NPs with Ponatinib (5mg, 10mg and 15mg) were prepared to determine the optimum concentration that will not cause any toxicity to the zebrafish embryos. The concentrations that have been prepared from each of the three groups by diluting the proper amount of the NPs in PTU are: 1, 0.75, 0.5, 0.25, 0.1, 0.05, 0.01, 0.005, 0.0025mg/ml. After that the PTU solution in the wells were removed and replaced it with the diluted NPs solution. The embryos were then incubated at 30°C and survival rate was measured at 48 hpf and 72 hpf. The surviving rate is calculated by dividing the number of the lived embryos over the total number of embryos multiplying by 100.

3.3.11 Xenograft exposure of loaded PLGA-PEG-PLGA NPs assay:

Injected 2-dpf zebrafish embryos have been allowed to recover for half an hour after injecting with K562 cells before exposing them to 0.001mg/ml loaded PLGA-PEG-PLGA NPs with 15mg and 10mg Ponatinib. The embryos have been separated in 6-well plate. Two wells for each group (control, 15mg and 10mg) with 10 embryos in each. The 0.001mg/ml concentration of loaded PLGA-PEG-PLGA NPs were prepared by diluting it in egg water. For a total of 3ml, the required amount for one well; a 1.440µl of the 15 and 10mg NPs was diluted in egg water. Then the embryos were incubated at 34°C and on 4-dpf embryos were imaged.

3.3.12 Survival rate analysis

At 48 hpf, the Dead embryos were removed from the 6-well cell culture plates to avoid influencing the surviving embryos during the toxicity experiments. The numbers of the dead, surviving and abnormal embryos of each NPs concentration groups were recorded until 3 dpf or 72 hpf. The surviving rate is calculated by dividing the number of the lived embryos over the total number of embryos multiplying by 100.

3.3.13 Cardiovascular structure/function analysis

To check for the cardiovascular toxicity of the unloaded and loaded NPs, the analysis was carried out at 3-dpf for the embryos in all the treated groups to see the influence of interference on cardiac function, structure and on the blood flow. The treated embryos were first fixed on a concave slide for imaging using 3% methyl cellulose. Under the Hamamatsu Orca high-speed camera and Zeiss Lumar V12 stereo microscope, images and high-speed time-lapse movies were recorded at about 100 fps for the heart and tail of each embryo through the HCImage software. Then to assess for the heart failure due to the toxicity of the nanoparticles, analysis of the gross cardiac structure for the presence of cardiac edema and major structural

defects such as looping defects was performed. Also, tail videos have been analyzed for the Red Blood Cells (RBCs) movement within the blood flow using the MicroZebraLab. Tracking the RBCs aids in measuring the blood velocity by following an in-house algorithm from Viewpoint for tracking RBCs. This algorithm has also used to measures heart rate in beats per minute that to calculate other cardiac function parameters such as cardiac output. Through extracting frames at end-diastole and end-systole points for calculating myocardial thickness and ventricular volumes. Increased myocardial thickness was associated with the presence of hypertrophy. Then the ventricular volumes at end-diastole and end-systole were determined to calculate several cardiac function parameters as outlined below. Assuming a prolate spheroidal shape, the following formula was used for ventricular volumes:

$$Volume = \frac{1}{6} \times \pi \times D_L \times {D_S}^2$$

Here, D_L and D_S are long-axis and short-axis diameters, respectively. Stroke volume (SV) is the blood volume pumped from the ventricle for each beat and is simply calculated from ventricle volumes at end-diastole and end-systole:

$$SV = (EDV - ESV)$$

Here EDV and ESV are end-diastole and end-systole volumes. Ejection fraction (EF) is defined as the fraction of blood ejected from the ventricle with each heartbeat:

$$EF\ (\%) = \frac{(EDV - ESV)}{EDV} \times 100 = \frac{SV}{EDV} \times 100$$

Cardiac output (CO) is the volume of blood being pumped by the heart. CO was calculated from SV and heart rate (HR) as follows:

CO (nanoliter/min) = SV (nanoliter/beat) × HR (beats/min)

FS is another measure of ventricular contractility. It was calculated from ventricle diameters at end-diastole and end-systole:

$$FS = \frac{(D_d - D_s)}{D_d}$$

3.3.14 Gene Expression via RT-PCR

The total RNA was isolated from 3dpf embryos treated with the TKIs (Ponatinib and Imatinib) and the control embryos by using the IBI DNA/RNA/Protein Extraction Kit **(**IBI Scientific -r IB47702) and following the manufacture instructions. Then the first-strand cDNA synthesis was done by following the manufacture instructions of the SuperScript™ IV VILO™ Master Mix kit (Thermo Fisher Scientific 11756050). After that, for the quantitative analysis of specific mRNA expression, Taqman real-time reverse transcriptase (Applied Biosystems®) and specific primers and probs that was designed and constructed (Applied Biosystems®) against the genes of interest; atrial natriuretic peptide (ANP) and brain natriuretic peptide (BNP) **Table (1)** have been used. The signal was read using the Real-Time PCR ABI 7500 System. While the relative quantity was calculated based on the 2-ΔCт method [86] and the fold change was calculated in reference to the control group.

Table 1: List of primers for RT-qPCR

Cataloge no.	Gene Name	RefSeq	Species
4331348	ANP – nppa zebrafish	NM_198800	Zebrafish
4331348	BNP – nppa zebrafish	NM_001327776	Zebrafish

3.3.15 Statistical analysis

Statistical analysis was performed using GraphPad Prism version 9 software. Data were analyzed using one way-ANOVA with Dunnet's multiple comparison test. A p-value of less than 0.05 was considered statistically significant. One asterisk (*) indicates $p<0.05$, two asterisk (**) indicates $p<0.01$, three asterisk (***) $p<0.001$ and four asterisk (****) indicates $p<0.0001$.

Chapter 4: Results

4.1 Fluorescent K562

Olympus fluorescent microscope was used to image the fluorescent K562 CML cells stained with CM-Dil fluorescent dye. The mCherry fluorescent filter with excitation/emission spectra of 587/610 has been chosen to examine the fluorescent K562 CML cells as the CM-Dil fluorescent dye has an excitation/emission of 553/570 nm maxima. **Figure (1)** represent an image of the fluorescent K562 cells at 60X magnification. As seen from the figure, most of the K562 cells were successfully fluorescently stained with CM-Dil dye.

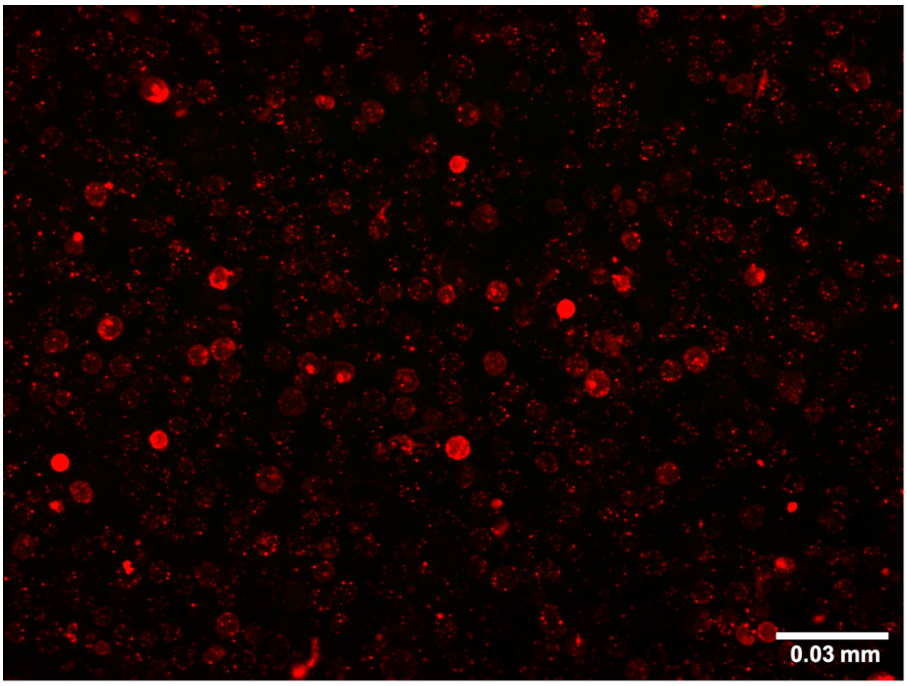

Figure 1: Fluorescently labelled K562.
Representative fluorescence images for K562 cells stained with CM-Dil dye (Red). Fluorescently labeled K562 cells at magnification 60X; Scale bar, 0.03mm.

4.2 PLGA-PEG-PLGA NPs characterization

4.2.1 PLGA-PEG-PLGA NPs morphology

TEM and SEM were used to characterize the shape of the PLGA-PEG-PLGA NPs. **Figure (2, A)** represents the shape of PLGA-PEG-PLGA NP, by TEM micrograph and it shows

the NPs with a round shape. **Figure (2, B)** represents the shape of PLGA-PEG-PLGA NPs using SEM indicating the NPs of spherical 3-dimensional.

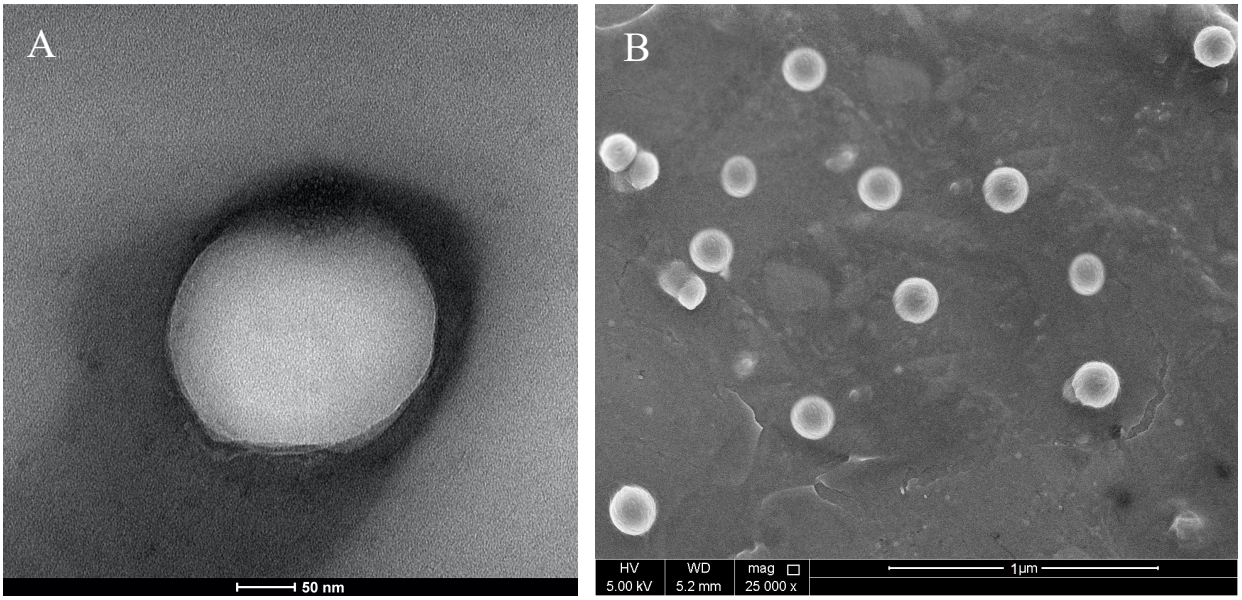

Figure 2: TEM and SEM micrographs of PLGA-PEG-PLGA NPs.
(A) TEM image of PLGA-PEG-PLGA Np on scale bar, 50 nm. **(B)** SEM image of PLGA-PEG-PLGA Nps on scale bar, 1µm.

4.2.2 PLGA-PEG-PLGA NPs size

The size of loaded PLGA-PEG-PLGA NPs with 5mg, 10mg and 15mg Ponatinib have been measured using the Nanosizer 2000-Malvern machine. The range of the NPs was around 80 to 100nm. The exact sizes of each NP group were, 74.55+/- 28.74 (d.nm)±SD for the PLGA-PEG-PLGA NPs loaded with 5mg Ponatinib **Figure (3, A)**, 125+/- 26.91 (d.nm)±SD for the PLGA-PEG-PLGA NPs loaded with 10mg Ponatinib **Figure (3, B)** and 116.9+/- 42.92 (d.nm)±SD for PLGA-PEG-PLGA NPs loaded with 15mg Ponatinib **Figure (3, C)**.

While the size of the unloaded PLGA-PEG-PLGA NPs was showed to be 84.33+/- 13.83 (d.nm)±SD **Figure (4)**. Indicating that PLGA-PEG-PLGA NPs have a size range approximately from 80 to 100nm and the loading of Ponatinib drug had showed to have a slight effect on the PLGA-PEG-PLGA NPs' size.

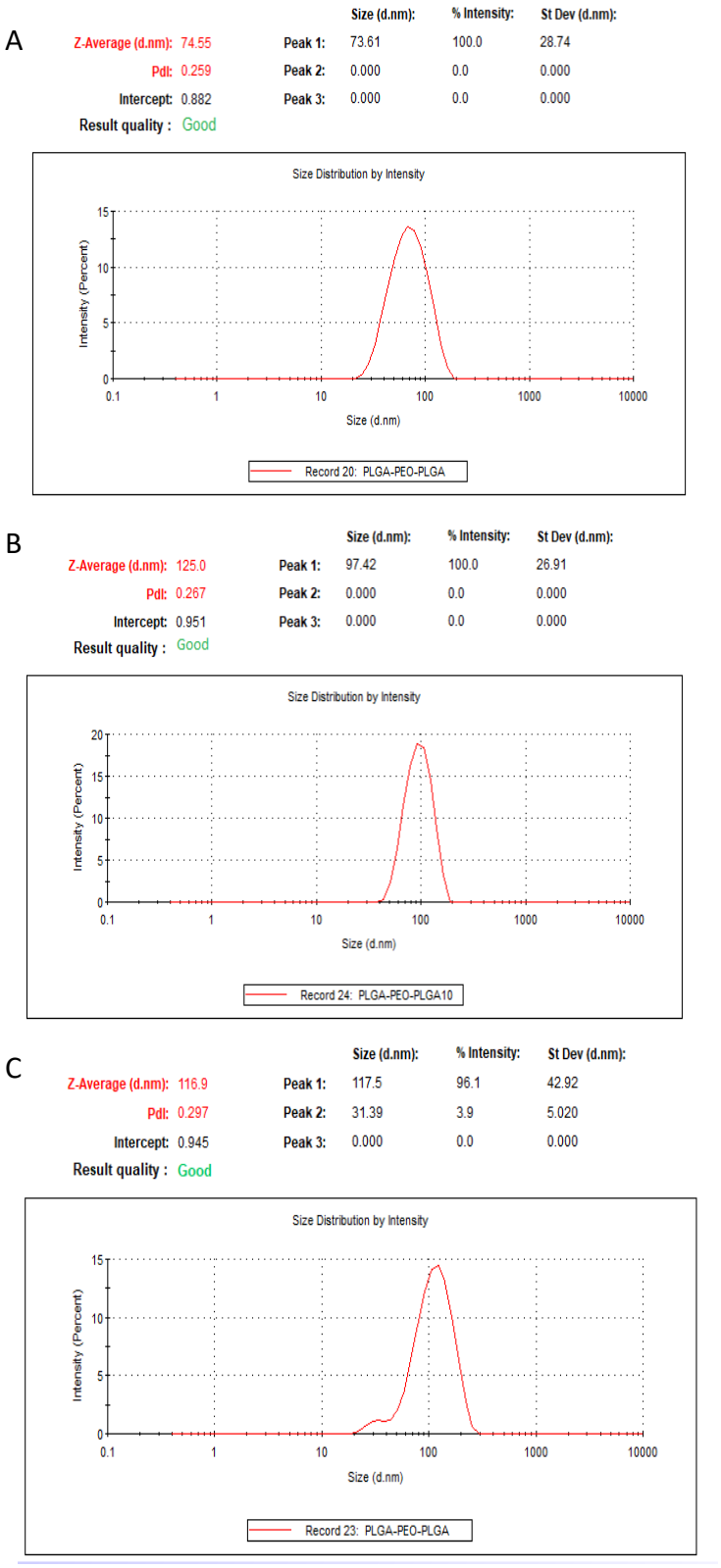

Figure 3: Ponatinib loaded PLGA-PEG-PLGA NPs intensity based particles size distribution.

Representative graphs of Nanosizer 2000-Malvern for loaded PLGA-PEG-PLGA NPs size **(A)** The size of PLGA-PEG-PLGA NPs loaded with 5mg Ponatinib is 74.55+/- 28.74 (d.nm)±SD **(B)** The size of PLGA-PEG-PLGA NPs loaded with 10mg Ponatinib is 125+/- 26.91 (d.nm)±SD **(C)** The size of PLGA-PEG-PLGA NPs loaded with 15mg Ponatinib is 116.9+/- 42.92 (d.nm)±SD.

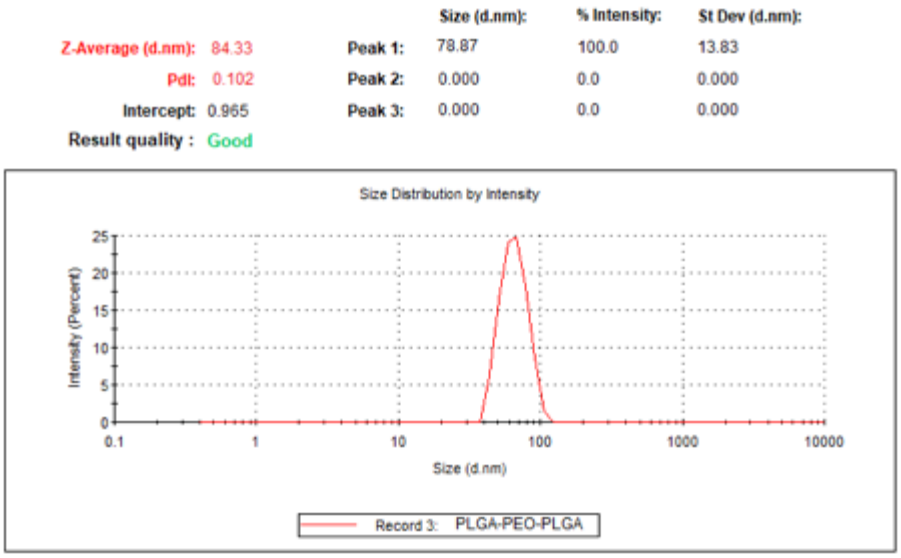

Figure 4 :Unloaded PLGA-PEG-PLGA NPs intensity based particles size distribution. Representative graph of Nanosizer 2000-Malvern for unloaded PLGA-PEG-PLGA NPs size. Size of unloaded PLGA-PEG-PLGA NPs is 84.33+/-13.83 (d.nm)±SD.

4.2.3 PLGA-PEG-PLGA NPs surface charge

The surface charge of the PLGA-PEG-PLGA NPs has been assessed to know more about the material properties, thus its interaction with the biological system can be predicted. For that, zeta potential for the loaded PLGA-PEG-PLGA NPs has been measured by the Nanosizer 2000-Malvern machine and the surface charge of the particles revealed to be positively charged as 12,3+/-5.5; 15,2+/-3.4 and 16,7+/-2.5 (mV)±SD for 15, 10 and 5mg PLGA-PEG-PLGA respectively **Table (2)**.

While the zeta potential for the unloaded PLGA-PEG-PLGA NPs have been measured by the ZetaSIZER NANO-Malvern hosted at the Center for Advanced Materials (CAM) at Qatar University. The particles surface charge revealed to be negatively charged with an average of -2.66+/-0.185 (mV)±SD **Table (3)**. The surface charge of the Ponatinib drug have also been measured which showed that the drug has a positive surface charge in an average of 30.86+/- 2.744(mV)±SD zeta potential **Table (4),** which seems to be the reason for changing of the surface charge of the particles when loaded with the drug.

Table 2: Loaded PLGA-PEG-PLGA NPs surface charge

	Sample name	Zeta Potential (mV) +/- STD
1	PLGA-PEG-PLGA NPs loaded with 5mg Ponatinib	16,7+/-2.5
2	PLGA-PEG-PLGA NPs loaded with 10mg Ponatinib	15,2+/-3.4
3	PLGA-PEG-PLGA NPs loaded with 15mg Ponatinib	12,3+/-5.5

Table 3: Unloaded PLGA-PEG-PLGA NPs surface charge

Sample Name	Zeta Potential (mV)
Unloaded Nano particles 1	-2.48
Unloaded Nano particles 2	-2.85
Unloaded Nano particles 3	-2.65
Mean	-2.66
STD	0.185

Table 4: Ponatinib drug surface charge

Sample Name	Zeta Potential (mV)
Ponatinib 1	32.5
Ponatinib 2	29.7
Ponatinib 3	33.7
Ponatinib 4	31.7
Ponatinib 5	26.7
Mean	30.86
STD	2.744

4.2.4 Ponatinib Dissolution Rate from PLGA-PEG-PLGA NPs

To determine the dissolution rate of Ponatinib drug, or the % of the released drug from the particles into the solution as a free drug, HPLC analysis of the dissolution samples from dissolution test have been performed. **Figure (5, A)** represent the standard graph of Ponatinib drug where it showed a peak at 1.678 retention time (RT).

Figure (5, B) of loaded PLGA-PEG-PLGA NPs with 5mg sample collected at 1 hour showed a clear peak at 1.699 RT indicating that Ponatinib have been released from the particles at the first hour. Although **Figure (5, C)**, which represent loaded PLGA-PEG-PLGA NPs with 5mg sample collected at 3 hours, has also showed a tiny peak at 1.699 RT, it was not significantly considered a clear release of the drug. While **Figures (5, D)** and **(5, E)** of loaded PLGA-PEG-PLGA NPs with 5mg sample collected at 5 hour and 24 hours respectively, did not showed any release of the drug in the buffer solution.

In the other hand, loaded PLGA-PEG-PLGA NPs with 10mg and 15mg samples did not show any release peak of the drug from the particles into the buffer at any time interval of 1hr, 3hr, 5hr 24hr and 48hr **Figure (5, F, G, H, I, J, K, L, M, N & O)**. Although there was a release of Ponatinib at the first hour from the 5mg PLGA-PEG-PLGA NPs, this rapid release is undesirable as this won't allow a longer circulation of the loaded NPs in vivo, but 10 and 15mg Ponatinib loaded PLGA-PEG-PLGA NPs did not show that, indicating the release of the drug could takes longer than 2 days and the drug is still inside and will travels with the NPs in vivo.

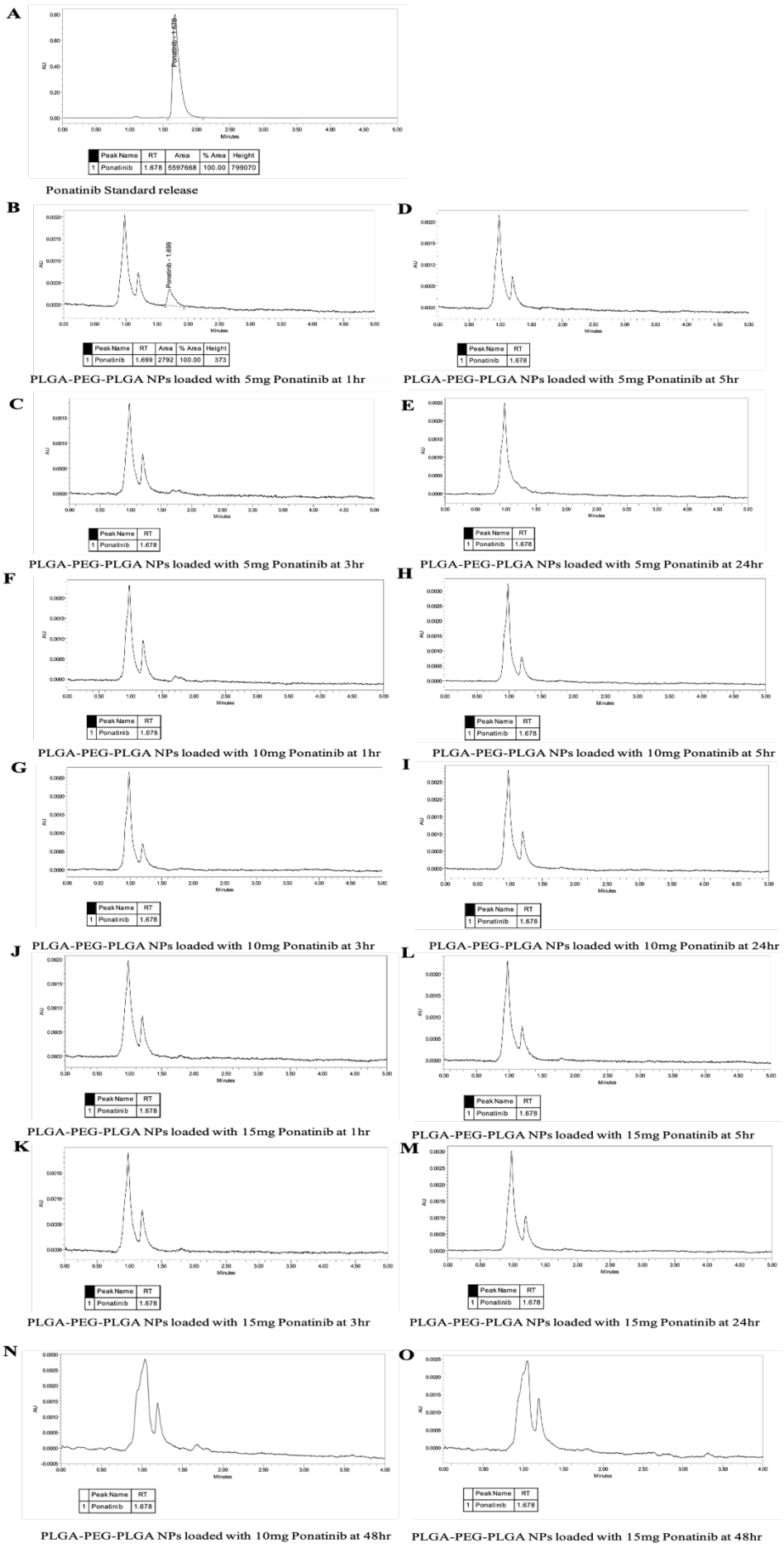

Figure 5: Ponatinib Dissolution Rate from PLGA-PEG-PLGA NPs.
Representative graphs of HPLC for Ponatinib Dissolution Rate from PLGA-PEG-PLGA NPs **(A)** Standard graph of Ponatinib drug peak at 1.678 RT. **(B)** PLGA-PEG-PLGA NPs loaded

with 5mg Ponatinib at 1hr. **(C)** PLGA-PEG-PLGA NPs loaded with 5mg Ponatinib at 3hr. **(D)** PLGA-PEG-PLGA NPs loaded with 5mg Ponatinib at 5hr. **(E)** PLGA-PEG-PLGA NPs loaded with 5mg Ponatinib at 24hr. **(F)** PLGA-PEG-PLGA NPs loaded with 10mg Ponatinib at 1hr. **(G)** PLGA-PEG-PLGA NPs loaded with 10mg Ponatinib at 3hr. **(H)** PLGA-PEG-PLGA NPs loaded with 10mg Ponatinib at 5hr. **(I)** PLGA-PEG-PLGA NPs loaded with 10mg Ponatinib at 24hr. **(J)** PLGA-PEG-PLGA NPs loaded with 15mg Ponatinib at 1hr. **(K)** PLGA-PEG-PLGA NPs loaded with 15mg Ponatinib at 3hr. **(L)** PLGA-PEG-PLGA NPs loaded with 15mg Ponatinib at 5hr. **(M)** PLGA-PEG-PLGA NPs loaded with 15mg Ponatinib at 24hr. **(N)** PLGA-PEG-PLGA NPs loaded with 10mg Ponatinib at 48hr. **(O)** PLGA-PEG-PLGA NPs loaded with 15mg Ponatinib at 48hr.

4.3 Ponatinib Toxicity

4.3.1 Survival Rate

Before, we assessed loaded nanoparticles, we first wanted to see how cardiotoxic Ponatinib is on zebrafish embryos. The survival rate of the zebrafish embryos at 24hr, 48hr and 72hr -post fertilizing (hpf) was calculated for the control, Ponatinib treated groups as well as for Imatinib as a first generation TKI. **Figure (6)** indicates that there is a significant decrease in the survival rate of 10µM and 5µM Ponatinib groups comparing to the normal and negative control groups (Control and 0.1%DMSO). Ponatinib was similarly cardiotoxic as Imatinib and the Ponatinib treated group with the lowest concentration (2.5µM) did not show any significant difference compared to the normal and negative control groups.

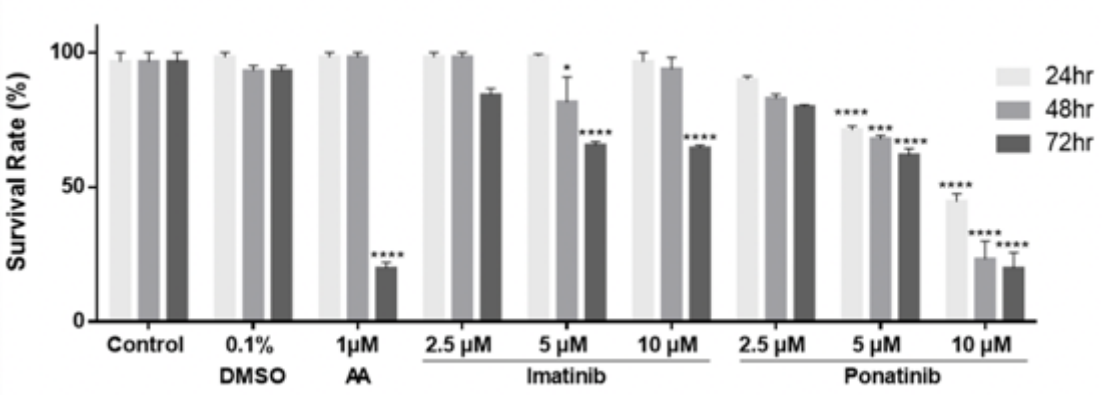

Figure 6: Ponatinib and Imatinib Survival Rate.
Survival rate of embryos exposed to different concentrations of Ponatinib and Imatinib compared to the PC (1µM AA) and NC, at different timepoint 24,48,72 hpf. n= 20, (*) = $p < 0.05$; (***) = $p < 0.001$, (****) = $p < 0.0001$.

4.3.2 Cardiovascular structure assessment

The cardiac structure was assessed by observing the morphological structure of the heart using the Hamamatsu Orca high-speed camera and Zeiss Lumar V12 stereo microscope. The embryos were photographed, and the phenotype of the treated group embryos were compared to the control and normal embryos **Figure (7, A).** For the treated group by the lowest concentration (2.5 and 5μM) of Imatinib **Figure (7, B & C),** the embryos heart showed to be normal but for the highest concentration (10μM) **Figure (7, D)** abnormal heart and size was shown. For Ponatinib (2.5 and 5μM) **Figure (7, E & F)** there was several abnormalities observed. This includes pericardial edema, lordosis or the combination of both. Edema has showed to be the most common among the embryos treated with Ponatinib and edema has showed to be causing cardiac abnormalities as the abnormal formation of the heart atrium and ventricle.

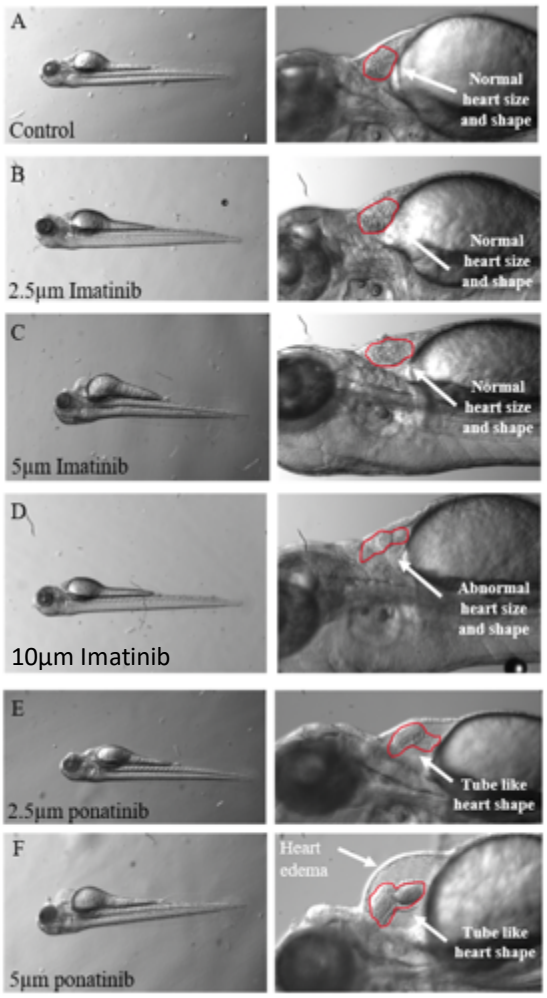

Figure 7: Embryo phenotypes following treatment with different concentrations of Imitinab and Ponitinab.
(**A**) DMSO (0.1%) treated embryos with normal heart size and shape. **(B)** Imatinib (2.5µM) treated embryos with normal heart size and shape, **(C)** Imatinib (5µM) treated embryos of normal heart size and shape. **(D)** Imatinib (10µM) treated embryos showed abnormal heart size and shape. **(E)** Ponatinib (2.5µM) and **(F)** Ponatinib (5µM) showed elongated tub-like structure heart and pericardial edema when compared to control.

4.3.3 Cardiac function assessment

The cardiac function was assessed by analyzing the dorsal aorta blood flow of the 2.5µM Ponatinib and Imatinib exposed groups. The aorta blood flow velocity of both TKIs significantly decreased compared to the normal and negative controls **Figure (8, A)**. The aorta diameter has also been reduced compared to the control groups **Figure (8, B)**. However, the aorta pulse did not show a significant difference between the groups **Figure (8, C)**.

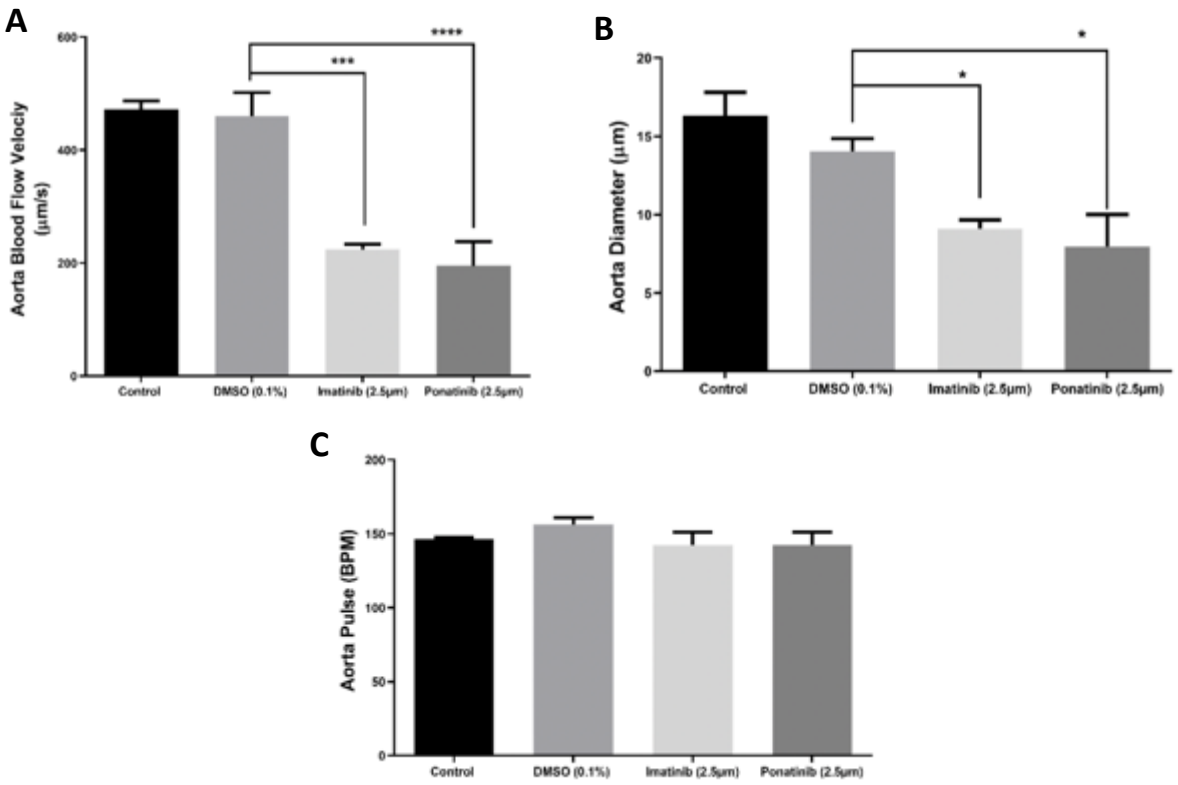

Figure 8: Ponatinib and Imatinib dorsal aorta blood flows analysis.
(A) Aorta blood flow velocity of Ponatinib and Imatinib (2.5µM) exposed embryos. **(B)** Aorta Diameter of Ponatinib and Imatinib (2.5µM) exposed embryos. **(C)** Aorta Pulse of Ponatinib and Imatinib (2.5µM) exposed embryos. (*) = $p < 0.05$; (***) = $p < 0.001$, (****) = $p < 0.0001$.

4.3.4 Cardiac markers gene expression

Ponatinib and Imatinib (2.5µM) have showed to be significantly increased the gene expression of atrial natriuretic peptide (*ANP*) and B-type natriuretic peptide (*BNP*) compared to the negative control (DMSO (0.1%)) indicating severe cardiotoxicity **Figure (9)**. Here AA is a well-known agent for heart failure, was used as a positive control. Ponatinib and Imatinib had similar cardiotoxicities. These findings clearly demonstrated that Ponatinib is associated with severe cardiotoxicity.

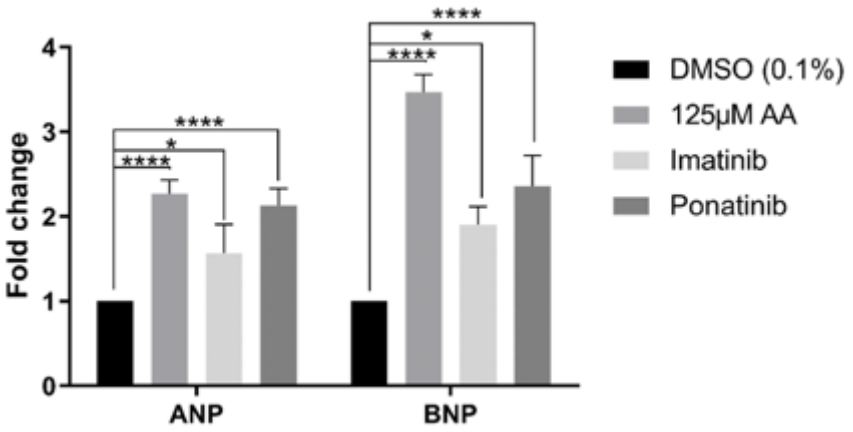

Figure 9: Gene expression fold changes in ANP and BNP cardiac markers.
The relative quantity was calculated based on the $2^{-\Delta C_T}$ method, and the fold change was calculated in reference to the control group. (*) = $p < 0.05$; (***) = $p < 0.001$, (****) = $p < 0.0001$.

4.4 Unloaded PLGA-PEG-PLGA NPs Toxicity

4.4.1 Survival rate

The survival rate of the zebrafish embryos at 72hr -post fertilizing (hpf) was calculated for the negative control (NC) and treated groups of unloaded PLGA-PEG-PLGA NPs. **Figure (10)** indicates that there is a significant decrease in the survival rate of 1.0 mg/ml group compared to the negative control group. While the experiment groups with the lowest concentration (0.75, 0.5, 0.25, 0.1 and 0.05 mg/ml) of unloaded PLGA-PEG-PLGA NPs did not showed any significant difference compared to the control group.

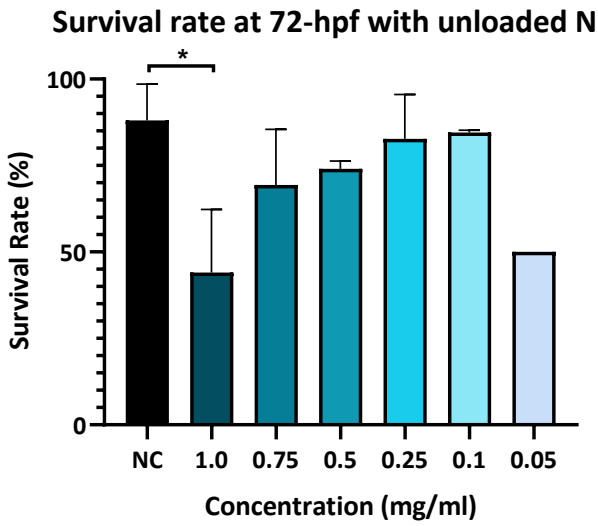

Figure 10: Unloaded PLGA-PEG-PLGA NPs Survival Rate.
Survival rate of embryos exposed to different concentrations of unloaded PLGA-PEG-PLGA NPs compared to the NC, at 72 hpf. (*) = $p < 0.05$.

4.4.2 Cardiac function assessment

The cardiac function was assessed by analyzing the heartbeat, the dorsal aorta (DA) and posterior cardinal vein (PCV) vessel diameter and blood flow velocity. The heartbeat of 0.75 mg/ml exposed group was significantly reduced compared to the negative control **Figure (11, A)**.

The dorsal aorta (DA) vessel diameter has been shown to be enlarged in groups (1.0, 0.5 and 0.25 mg/ml) and the blood velocity was increased significantly in the 0.25 mg/ml group compared to the negative control **Figure (11, B & C)**.

In the posterior cardinal vein (PCV) the vessel diameter has been shown to be enlarged in groups (0.5, 0.25, 0.1 mg/ml) and the blood velocity was also seen to be increased significantly in the 0.25 mg/ml group **Figure (11, D & E)**. Based on these results, only high concentration of unloaded NPS seem to be toxic to the animals.

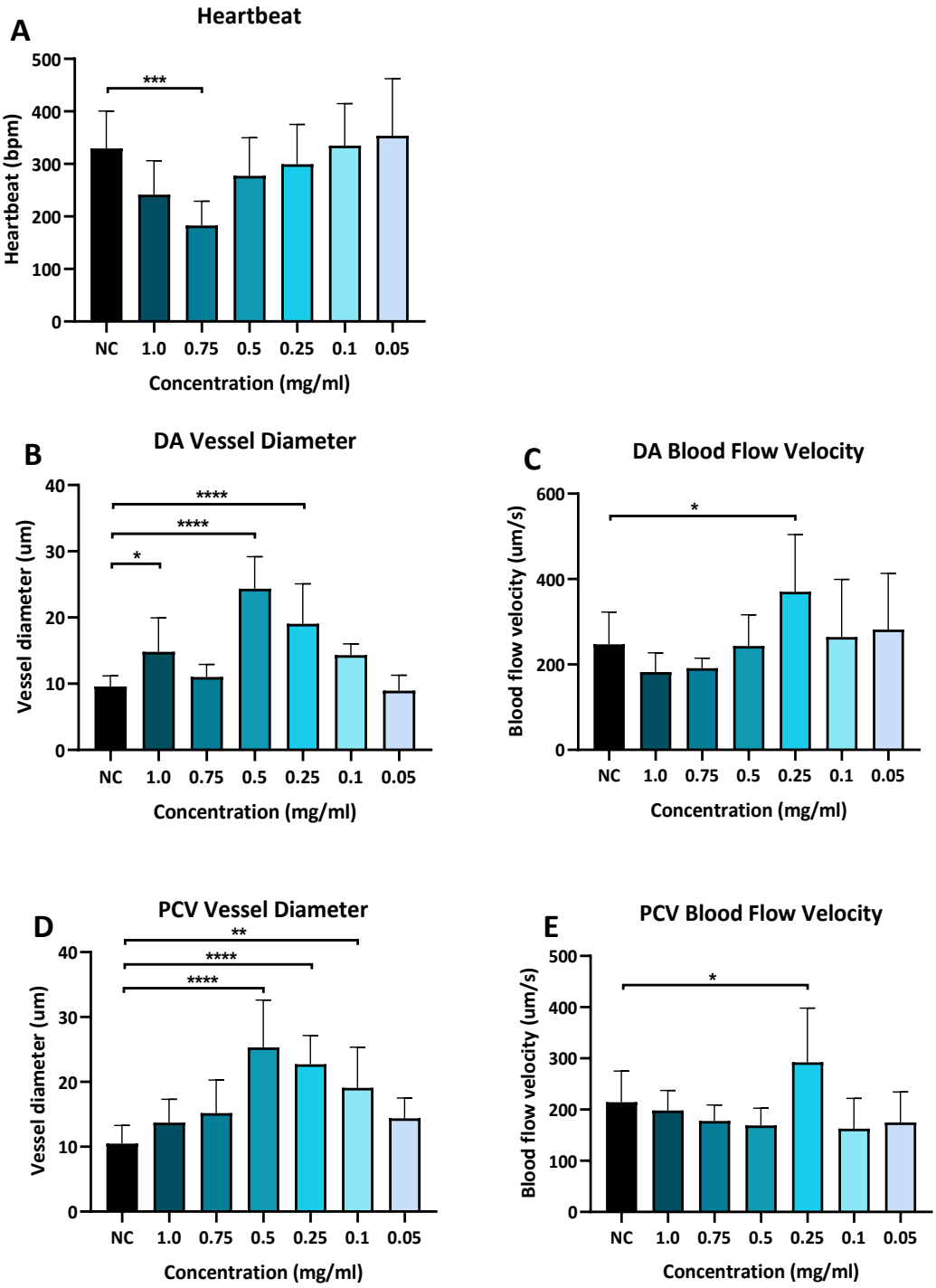

Figure 11: Cardiac function assessment of unloaded PLGA-PEG-PLGA.
(A) Heartbeat of embryos exposed to different concentrations of unloaded PLGA-PEG-PLGA NPs. **(B)** DA vessel diameter of embryos exposed to different concentrations of unloaded PLGA-PEG-PLGA NPs. **(C)** DA blood flow velocity of embryos exposed to different concentrations of unloaded PLGA-PEG-PLGA NPs. **(D)** PCV vessel diameter of embryos exposed to different concentrations of unloaded PLGA-PEG-PLGA NPs. **(E)** PCV blood flow

velocity of embryos exposed to different concentrations of unloaded PLGA-PEG-PLGA NPs. (*) = $p < 0.05$; (***) = $p < 0.001$, (****) = $p < 0.0001$.

4.5 Loaded PLGA-PEG-PLGA NPs Toxicity

4.5.1 Survival rate

The survival rate of the zebrafish embryos at 72hr -post fertilizing (hpf) was calculated for the negative control and treated groups of loaded PLGA-PEG-PLGA NPs with 5, 10 and 15mg Ponatinib. **Figure (12, A)** of the of loaded PLGA-PEG-PLGA NPs with 5mg Ponatinib indicates that higher concentrations of the loaded PLGA-PEG-PLGA NPs (1 and 0.75 mg/ml) have the lowest survival rate compared to the other groups. **Figure (12, B)** of the of loaded PLGA-PEG-PLGA NPs with 10mg Ponatinib showed that 1 and 0.5 mg/ml groups have the lowest survival rate. And **Figure (12, C)** of the of loaded PLGA-PEG-PLGA NPs with 15mg Ponatinib also showed that 1 and 0.75 mg/ml exposed groups have the lowest survival rate compared to the other groups.

Based on these results, only high concentration of loaded NPs seems to be toxic to the animals and the concentration of 0.001 mg/ml in 10 and 15mg Ponatinib loaded NPs showed to have similar survival rate to the negative control providing that this concentration is the most optimum than the others. While the concentration of 0.001 in 5mg did not show similar results that this could be due to the initial release of the drug in vivo.

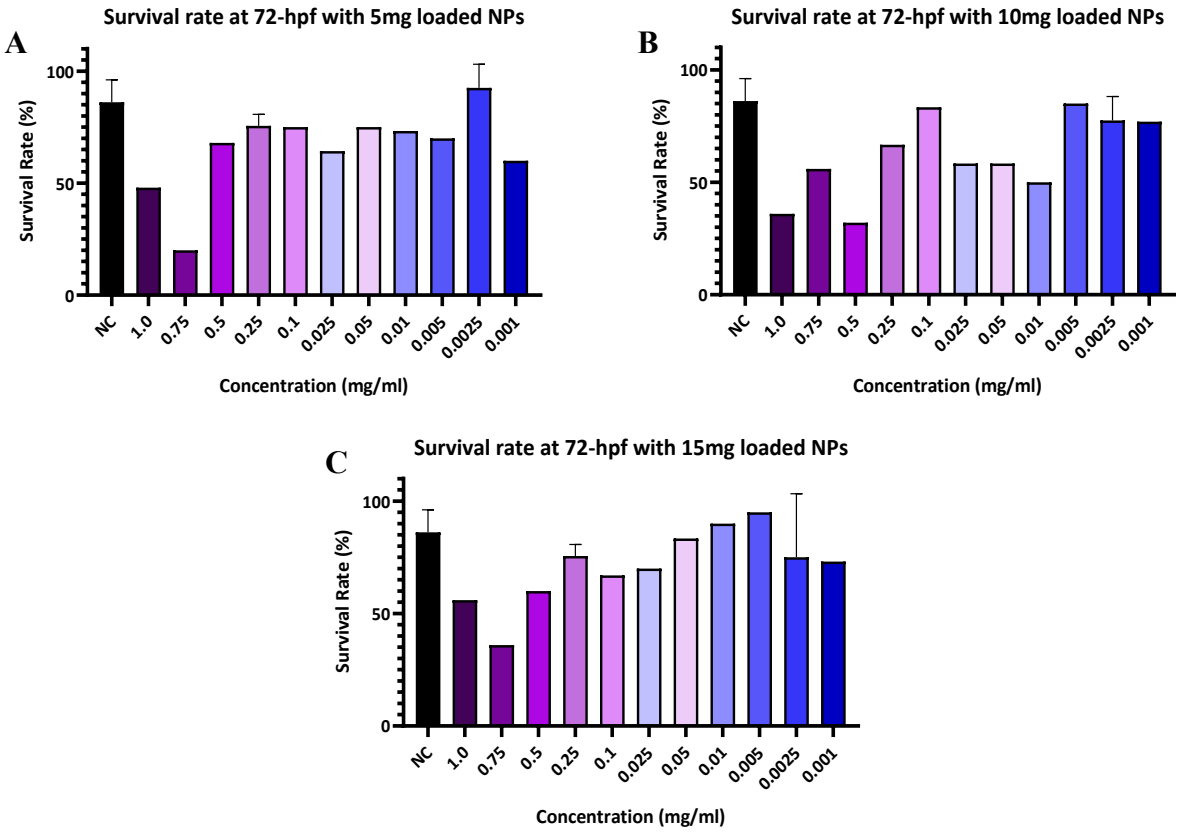

Figure 12: Loaded PLGA-PEG-PLGA NPs Survival Rate.
(A) Survival rate of embryos exposed to different concentrations of 5mg Ponatinib loaded PLGA-PEG-PLGA NPs compared to the NC, at 72 hpf. **(B)** Survival rate of embryos exposed to different concentrations of 10mg Ponatinib loaded PLGA-PEG-PLGA NPs compared to the NC, at 72 hpf. **(C)** Survival rate of embryos exposed to different concentrations of 15mg Ponatinib loaded PLGA-PEG-PLGA NPs compared to the NC, at 72 hpf. (*) = $p < 0.05$.

4.5.2 Cardiac function assessment

The cardiac function was assessed by analyzing the heartbeat, the dorsal aorta (DA) and posterior cardinal vein (PCV) vessel diameter and blood flow velocity. The heartbeat of groups 5mg; 0.005 and 0.0025mg/ml, 10mg; 0.005, 0.0025 and 0.001mg/ml and 15mg; 0.0025 and 0.001 mg/ml were significantly reduced compared to the negative control **Figure (13, A)**.

The dorsal aorta (DA) vessel diameter has been shown to be enlarged in all the testable groups 5mg (0.005 and 0.0025mg/ml), 10mg (0.0025mg/ml) and 15mg (0.0025 and

0.001mg/ml). And the blood velocity was significantly reduced in 15mg (0.005mg/ml) and high but not significantly in 15mg (0.0025mg/ml) **Figure (13, B & C)**.

In the posterior cardinal vein (PCV) the vessel diameter has been shown to be significantly enlarged in 5mg (0.0025mg/ml), 10mg (0.005, 0.0025, 0.001mg/ml) and 15mg (0.005, 0.0025, 0.001 mg/ml) the blood velocity was significantly reduced in 15mg (0.005mg/ml) **Figure (13, D & E)**.

According to these results 0.001 mg/ml from both 10mg and 15 mg concentrations seem to be non-toxic, and these would be used further in the xenograft experiments since targeting the cancer cells with highest drug concentration is possible by limiting toxicity.

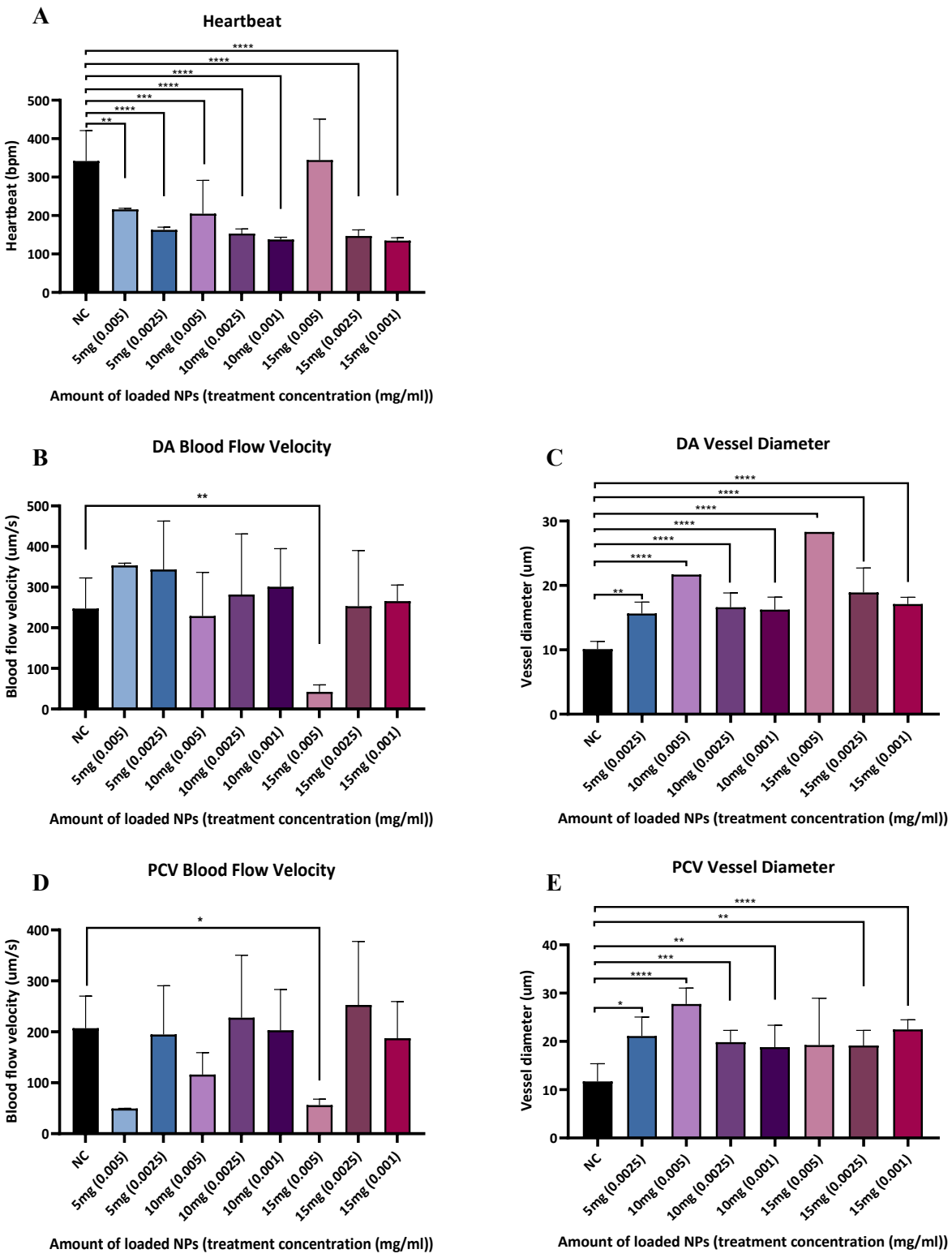

Figure 13: Cardiac function assessment of loaded PLGA-PEG-PLGA NPs.
(A) Heartbeat of embryos exposed to different concentrations of loaded PLGA-PEG-PLGA NPs with 5, 10 or 15mg Ponatinib. **(B)** DA blood flow velocity of embryos exposed to different concentrations of loaded PLGA-PEG-PLGA NPs with 5, 10 or 15mg Ponatinib. **(C)** DA vessel diameter of embryos exposed to different concentrations of loaded PLGA-PEG-PLGA NPs with 5, 10 or 15mg Ponatinib. **(D)** PCV blood flow velocity of embryos exposed to different

concentrations of loaded PLGA-PEG-PLGA NPs with 5, 10 or 15mg Ponatinib. **(E)** PCV vessel diameter of embryos exposed to different concentrations of loaded PLGA-PEG-PLGA NPs with 5, 10 or 15mg Ponatinib. (*) = $p < 0.05$; (***) = $p < 0.001$, (****) = $p < 0.0001$.

4.6 Zebrafish Xenograft Model

K562 CML cell line was successfully transplanted into the 72-hpf zebrafish embryos. **Figure (14)** represents a xenografted embryo from one day post injection to three days post injection (dpi) compared to a negative control embryo to differentiate between the autofluorescence of the embryos. The fluorescently labeled cancer cells with CM-Dil red fluorescent dye have been seen to increase in mass and spread into further sites of the embryo over time as indicated by the white arrows. The yolk sac area (white X) which was the injection site of the cells, showed the most tumor mass. Also, cancer cells showed to circulate through the blood into other parts of the embryos, as seen in the embryo eyes (white Y) and tail (white Z).

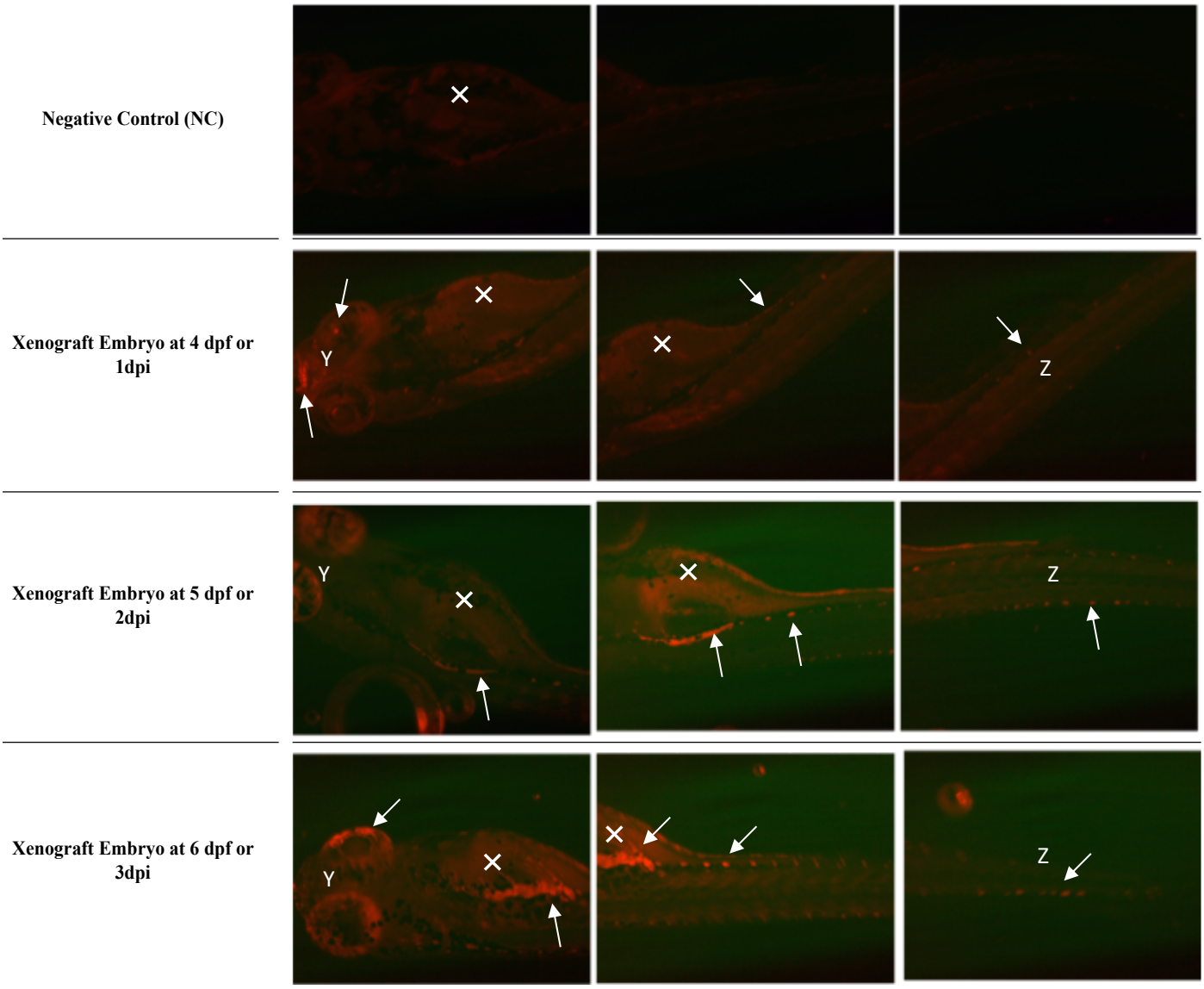

Figure 14: Zebrafish Xenograft model injected at 3 dpf.
Zebrafish screening at 4 dpf to 6 dpf using fluorescent microscopy and investigation of fluorecent K562 cells proliferation (White solid arrows) through out the animal body (Y: eyes, X: yolk sac, Z: tail) using mCherry fluorescence filter.

K562 CML cell line was also successfully transplanted when injected into the 48-hpf zebrafish embryos. **Figure (15)** represent a xenografted embryo from one day post injection to five days post injection (dpi) compared to a negative control embryo to differentiate between the autofluorescence of the embryos. The fluorescently labeled cancer cells have been seen to increase in mass and circulate into further sites of the embryo over time as indicated by the white arrows. The yolk sac area (white X) which was the injection site of the cells also showed the most tumor mass. And the cells have also showed to circulate through the blood as seen in the embryo eyes (white Y) and tail (white Z).

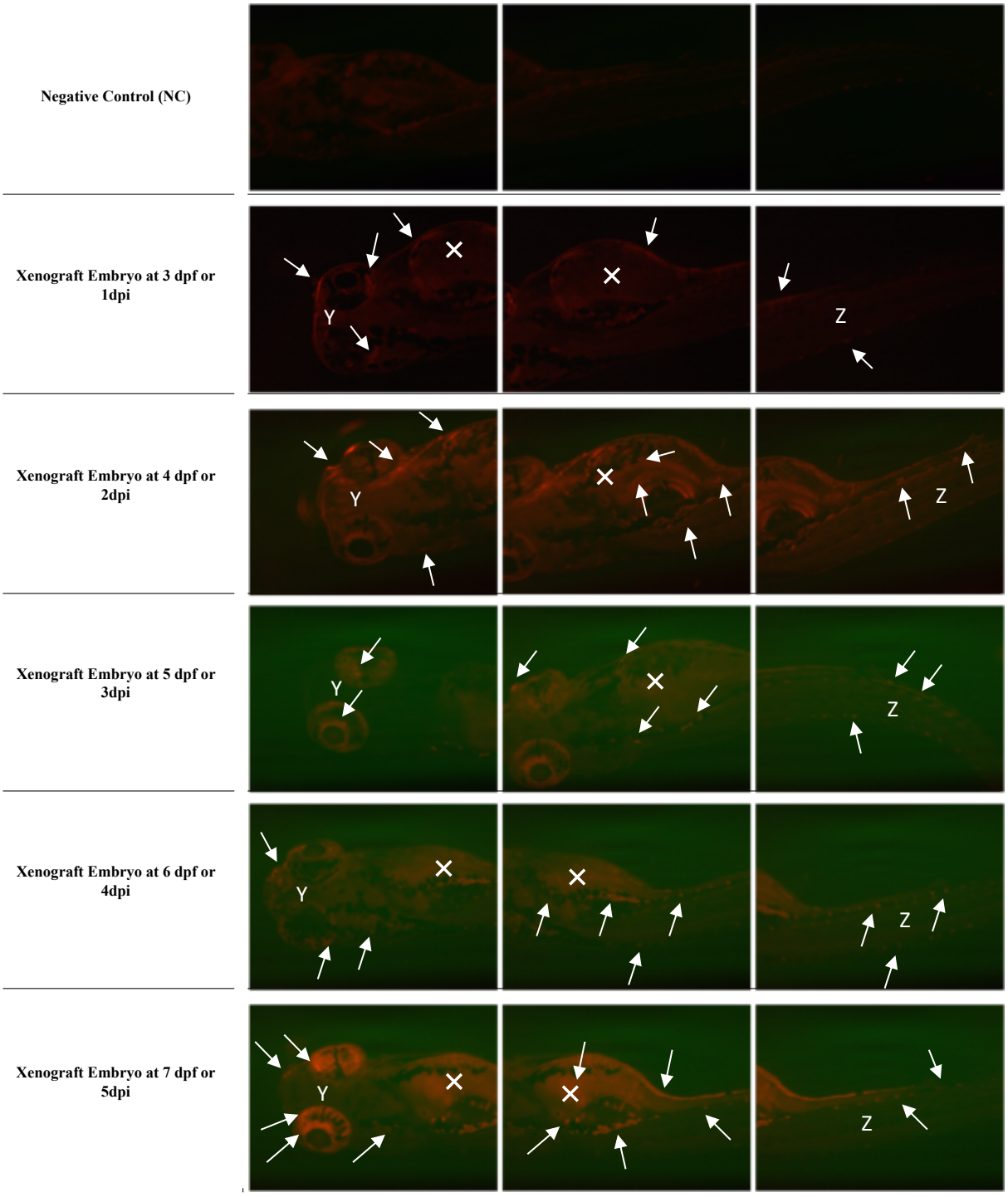

Figure 15: Zebrafish Xenograft model injected at 2 -dpf.
Zebrafish screening at 3 dpf to 7 dpf using fluorescent microscopy and investigation of fluorecent K562 cells proliferation (White solid arrows) through out the animal body (Y: eyes, X: yolk sac, Z: tail) using mCherry fluorescence filter.

4.7 Xenograft model exposed to loaded PLGA-PEG-PLGA NPs

Loaded PLGA-PEG-PLGA NPs with 10mg Ponatinib of 0.001mg/ml concentration

have been used to be exposed to the 2dpf xenograft embryos at the same day of the cancer cells injection. **Figure (16)** represent a xenografted embryo from two-day post injection and NPs exposure to five days post injection (dpi) and NPs exposure compared to a negative control embryo. The fluorescently labeled cancer cells have been seen to increase in mass and circulate into further sites of the embryo over time as indicated by the white arrows. The yolk sac area (white X) which was the injection site of the cells also showed the most tumor mass. And the cells have also showed to circulate through the blood as seen in the embryo eyes (white Y) and tail (white Z), indicating that the loaded NPs are taking long time to release Ponatinib, as shown that there was no obvious decrease in tumor cells mass.

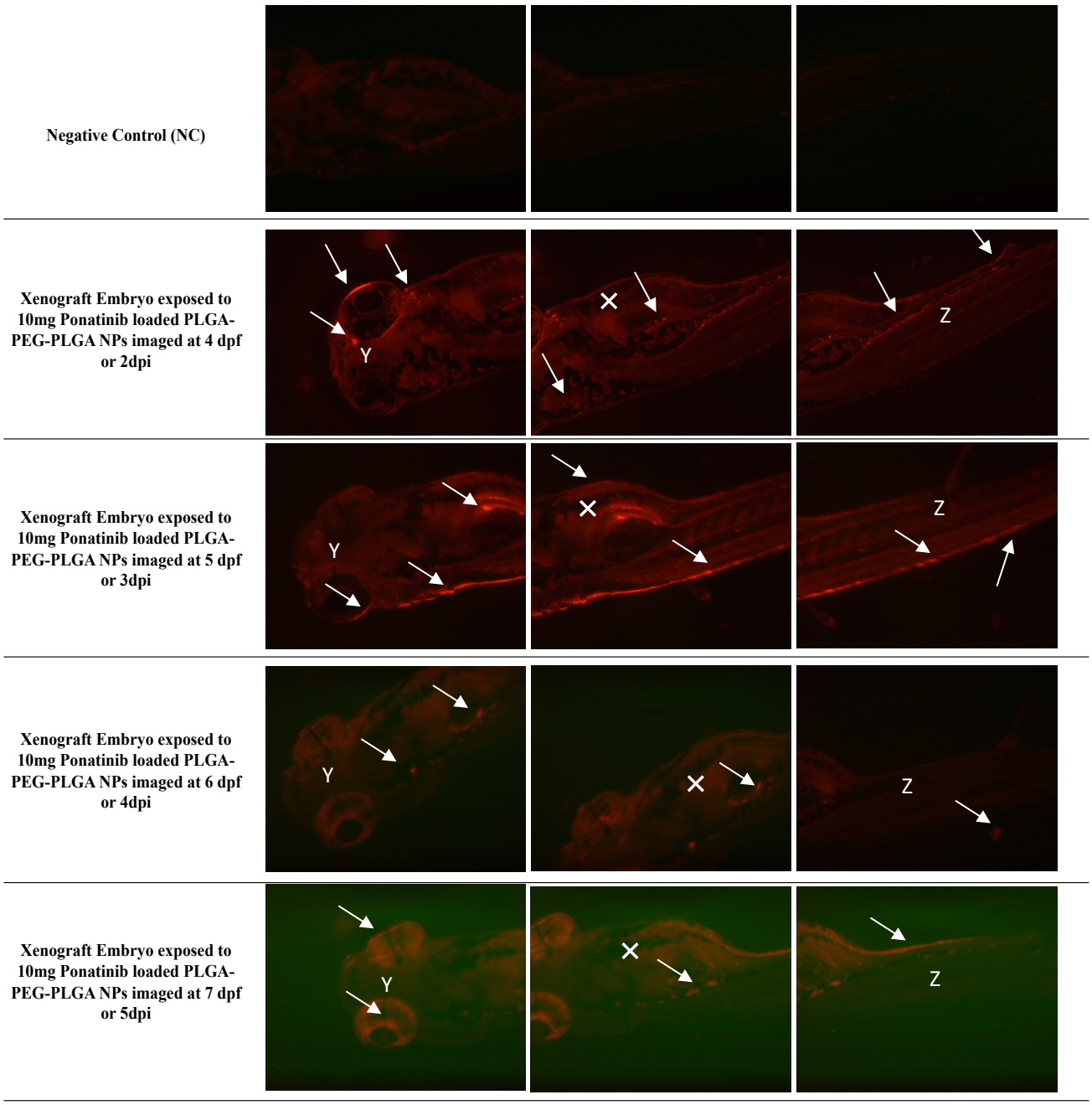

Figure 16: Xenograft model exposed to loaded PLGA-PEG-PLGA NPs with 10mg Ponatinib.

Zebrafish screening at 4 dpf to 7 dpf using fluorescent microscopy and investigation of fluorecent K562 cells proliferation (White solid arrows) through out the animal body (Y: eyes, X: yolk sac, Z: tail) using mCherry fluorescence filter after exposing zebrafish embryos to 0.001mg/ml of loaded PLGA-PEG-PLGA NPs with 10mg Ponatinib.

Also, loaded PLGA-PEG-PLGA NPs with 15mg Ponatinib of 0.001mg/ml concentration have been used to be exposed to the 2dpf xenograft embryos at the same day of the cancer cells injection. **Figure (17)** represent a xenografted embryo from two-day post injection and NPs exposure to five days post injection (dpi) and NPs exposure compared to a negative control embryo. The fluorescently labeled cancer cells have been seen to increase in mass and circulate into further sites of the embryo over time as indicated by the white arrows. The yolk sac area (white X) which was the injection site of the cells also showed the most tumor mass. And the cells have also showed to circulate through the blood as seen in the embryo eyes (white Y) and tail (white Z),indicating that the loaded NPs are taking long time to release Ponatinib, as shown that there was no obvious decrease in tumor cells mass.

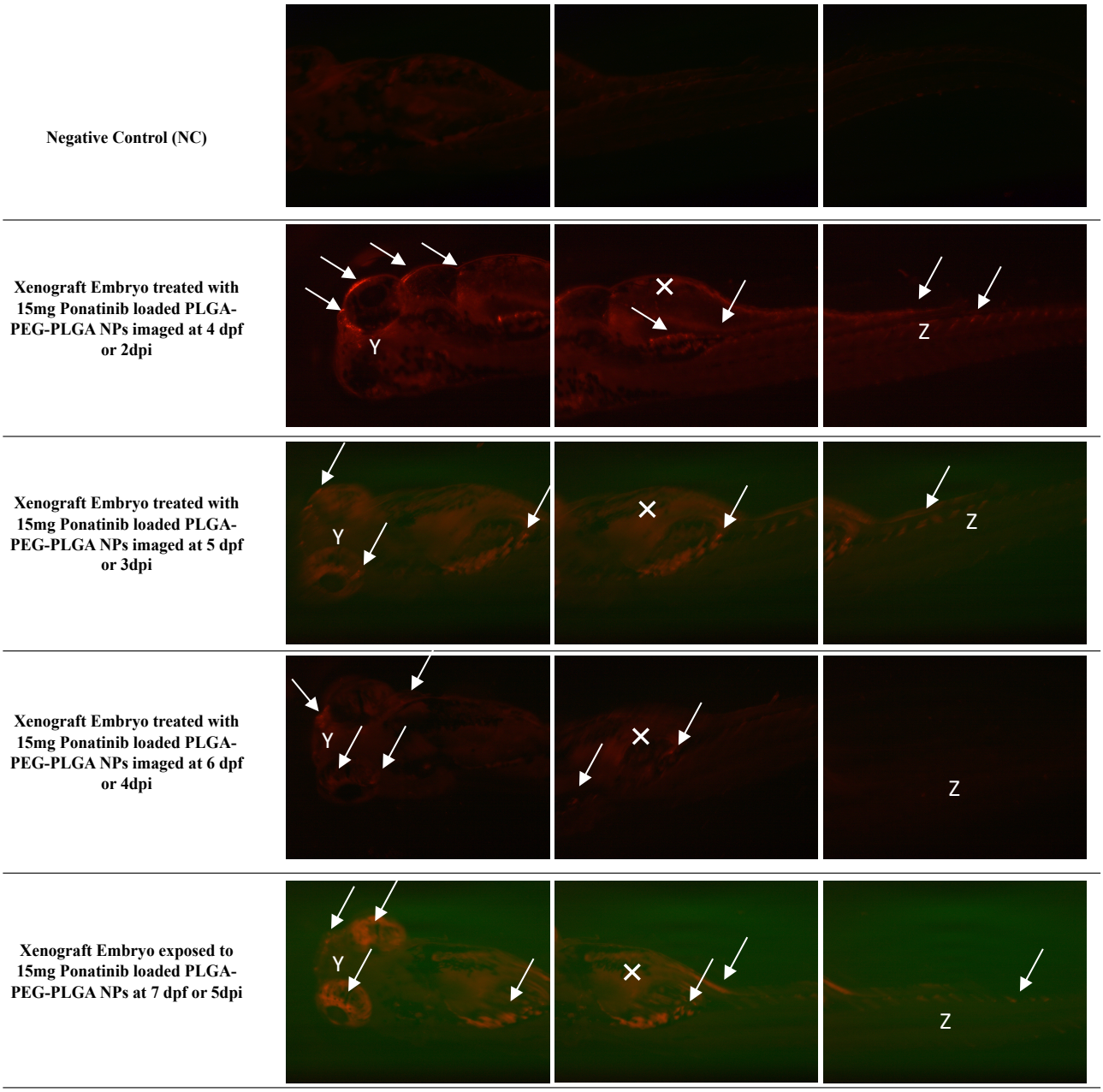

Figure 17: Xenograft model exposed to loaded PLGA-PEG-PLGA NPs with 15mg Ponatinib. Zebrafish screening at 4 dpf to 7 dpf using fluorescent microscopy and investigation of fluorecent K562 cells proliferation (White solid arrows) through out the animal body (Y: eyes, X: yolk sac, Z: tail) using mCherry fluorescence filter after exposing zebrafish embryos to 0.001mg/ml of loaded PLGA-PEG-PLGA NPs with 15mg Ponatinib.

4.8 Loaded PLGA-PEG-PLGA NPs uptake

Figure (18) showed the successful uptake of the fluorescence labeled loaded PLGA-PEG-PLGA NPs with 10 or 15mg Ponatinib after 2dpi or 2 days after treatment comparing to the negative control. The loaded PLGA-PEG-PLGA NPs were stained by 5DTAF a green fluorescence colored dye, that have been seen under the GFP filter. White arrows are showing the fluorescence labeled NPs in through the embryo's eye (white Y), yolk sac (white X) and tail (white Z).

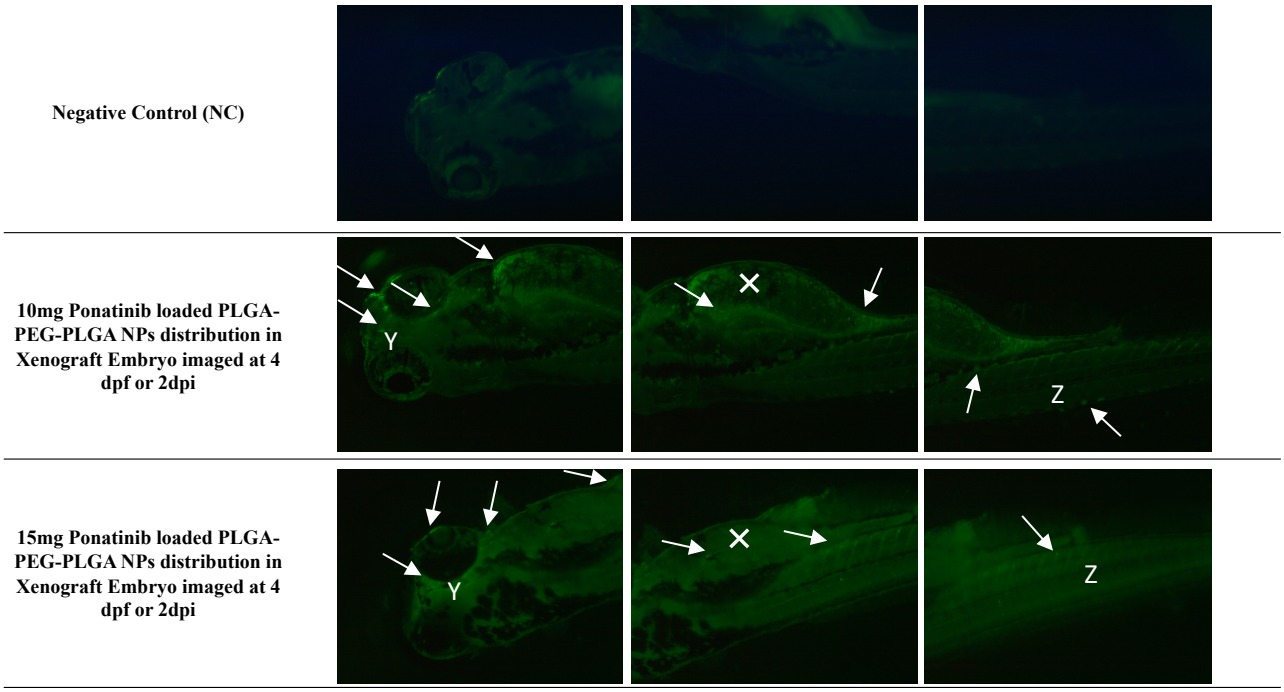

Figure 18: Loaded PLGA-PEG-PLGA NPs uptake.
Zebrafish screening at 4 dpf using fluorescent microscopy and investigation of fluorecent PLGA-PEG-PLGA NPs distribution (White solid arrows) through out the animal body (Y: eyes, X: yolk sac, Z: tail) using GFP fluorescence filter.

Chapter 5: Discussion

As cancer is one of the main causes of death worldwide, many research studies are currently focusing on finding new and efficient therapies to reduce side effects associated with conventional therapies of cancer [87]. Nanomedicine is one of the new approaches to overcome the cancer conventional therapies related issues such as, the low bioavailability and low specificity of the cancer drugs or contrast agents [88]. Thus, encapsulating the anti-cancer drugs or the active agents in nanoparticles would increase their biocompatibility, solubility, stability in body fluids and their retention time in tumor vasculature which would enhance the efficacy of the treatment [89-91].

Moreover, nanomedicine could also aid in cardio-oncology which is an inter-disciplinary field of studying, detection and treating cardiovascular adverse effects due to cancer therapies [92]. Although, TKIs are effective and preferred choice of therapy in several kind of cancers, such as CML, their toxicity remains a major concern particularly the cardiotoxicity in the cancer patients [70]. Therefore, in this study the TKI, Ponatinib has been loaded into the PLGA-PEG-PLGA NPs in order to enhance the anti-cancer efficacy and reduce cardiotoxicity related to TKIs.

First of all, to determine the cardiotoxicity of the anti-cancer TKI drug i.e., Ponatinib, the zebrafish model has been used in this study due to the transparency of the zebrafish embryos that allows a non-invasive examination of the organ development and toxic end points of the tested drugs [93]. The cardiotoxicity was determined by the morphological structure and by measuring the survival rate, cardiac outputs and atrial natriuretic peptide (*ANP*) and B-type natriuretic peptide (*BNP*) mRNA expression. Ponatinib has showed the most cardiotoxicity compared to the other TKI i.e., Imatinib with abnormal heart size and shape and the presence of pericardial edema. The aorta diameter, blood flow velocity and aorta cardiac output were significantly reduced. Also, the atrial natriuretic peptide (ANP) and B-type natriuretic peptide (BNP) showed a significant high

fold change compared to the normal control, and these natriuretic peptides play many important roles such as regulating blood pressure and blood volume, in regulating the permeability of the systemic vasculature, cellular proliferation and growth [94]. Also, BNP and ANP are the most common used diagnosed markers for heart failure [95].

This cardiotoxicity of Ponatinib has also seen by other previous studies who tested Ponatinib on the zebrafish model. For instance, Singh et. al. (2019), has used the BNP reporter line of the transgenic zebrafish and they have reported that Ponatinib showed the most cardiotoxicity compared to other CML TKIs by inhibiting cardiac pro-survival signaling pathways AKT and the extracellular signal regulated kinase (ERK) as well as to induce cardiomyocyte apoptosis [96]. While Zhu et. al. (2020), has used Ponatinib to induce ischemic stroke model of zebrafish indicating that the pathophysiology Ponatinib in inducing ischemic stroke is similar to that of ischemic stroke in humans [97].

Secondly, the smart nanoparticle PLGA-PEG-PLGA NPs has been synthesized through mixing the organic solution (PLGA- PEG- PLGA polymers, fluorescently labeled PLGA and THF) with the water solution (Pluronic F127 and milli Q water). The PLGA-PEG-PLGA NPs characteristics (size, shape and surface charge) have been studied. The size of the empty PLGA-PEG-PLGA NPs showed to be 84.33nm. However, Sulaiman et. al. (2019) has shown that the PLGA- PEG- PLGA NPs size is in the range of 206 to 402 nm, demonstrating that the experimental design for preparing PLGA-PEG-PLGA polymers has effects on the polymers size [98]. SEM has showed the NPs to be spherical in 3- dimensions with smooth surface. This is because SEM is used to examine material surfaces and it's based on scattered electrons [99]. While, TEM showed the NPs to be round of clear internal elements, TEM was used to show the NPs in a higher magnification as it's based on transmitted electrons and it has a higher electron energies than SEM

that allows them to penetrate through the particles to define any internal elements in the particles [99]. Moreover, the surface charge of the empty PLGA-PEG-PLGA NPs has been determined by measuring the zeta potential that would aid in determining more about the particle properties and its interaction with the biological system. The empty PLGA-PEG-PLGA NPs revealed to have negatively charge surface (-2.66mV) as the polymer is affected by the PLGA co-polymer end group [98].

In addition, the cardiotoxicity of empty PLGA-PEG-PLGA NPs have been studied to determine if this type of polymers would cause any cardiotoxicity or adverse side effects. To test for them, zebrafish model has also been used and the high concentrations of PLGA-PEG-PLGA NPs (1 mg/ml & 0.75 mg/ml) showed to have a little toxicity as indicated by the low survival rate than the normal control and by the cardiac outputs with low heartbeat, low DA diameter and blood flow velocity. While the lowest concentrations (0.5, 0.25, 0.1 and 0.05 mg/ml) showed values close to that of the normal control, showing that PLGA-PEG-PLGA NPs has low toxic effects as these PLGA-PEG-PLGA NPs have been approved by the US Food and Drug Administration due to their excellent biodegradability and because of their ability to improve bioavailability and antitumor targeting [100-102].

Thirdly, the smart nanoparticle PLGA-PEG-PLGA has been loaded with 5mg, 10mg or 15mg Ponatinib in order to reduce the drug side toxicity especially on the cardiovascular system. The loading of the drug was successfully performed, and this was indicated by the change in the surface charge of the PLGA-PEG-PLGA NPs from negative (-2.66mV) to positive (12.3, 15.2 and 16.7mV) charge for 15mg, 10mg and 5mg, respectively through measuring the zeta potential. This is because the Ponatinib surface charge is positive (30.86 mV). This phenomenon was also seen by Ku et al. (2010), who disclosed the change in the FMSNs surface charge from negative (-22.43

mV) to positive (18.93 mV) due to the conjugation of PAMAM of a positive charge and eventually the charged change almost to neutral (1.49 mV) revealing an additional modification of PEG [103]. Moreover, the HPLC analysis has confirmed the presence of Ponatinib in the PLGA-PEG-PLGA NPs particularly in the PLGA-PEG-PLGA NPs loaded with 5mg Ponatinib at 1hr, with a peak at 1.699 RT and this has been seen at 3hr but the peak was too small to be definitely defined as ponatinib. However, this initial burst release of the drug within a short period of time is undesirable as it would shorten the drug overall therapeutic duration and toxicity could also be associated in case of excessive burst release [104]. Therefore, PLGA-PEG-PLGA NPs loaded with 10mg and 15mg that did not show any burst release over the period of two days are the better choice for in vivo testing.

Fourthly, before testing for the efficacy of those loaded PLGA-PEG-PLGA NPs with 10 and 15mg Ponatinib, in reducing the cardiotoxicity and as effective anti-cancer therapy to treat CML, their cardiotoxicity has also been determined using the zebrafish embryos. The concentration of 1, 0.75, 0.5, 0.25, 0.1, 0.025, 0.05 and 0.01mg/ml of all groups (5, 10 and 15mg) had showed a very clear toxicity based on their survival rates which were the lowest and their morphology that was similar to the toxicity results of the Ponatinib drug as the embryos were deformed with heart edema and abnormal heart structure as well as for the absence of blood flow in the PCV and DA. This could be due to the burst release of Ponatinib that has been determined to cause cardiotoxicity or could be due to the presence of free Ponatinib in the stock vial of the PLGA-PEG-PLGA NPs. However, the lowest concentrations (0.005 and 0.0025mg/ml) had showed a better effect but still there was some observed abnormalities in the embryos, thus the 5mg Ponatinib loaded PLGA-PEG-PLGA NPs were excluded and a lower concentration (0.001mg/ml) from 10 and 15mg Ponatinib loaded PLGA-PEG-PLGA NPs has been tested and it

has showed the best results with better survival rate, morphology and cardiac output.

After that, a zebrafish xenograft model has been generated to test for the efficacy of those loaded PLGA-PEG-PLGA NPs with 10 and 15mg Ponatinib, in reducing the cardiotoxicity and as effective anti-cancer therapy to treat CML. This was done by transplanting the human K562 cell line. This xenograft model has also been successfully generated as indicated by the spread of the tumor cells over the period of 6 days post injection and this model was also achieved by previous studies. For example, Corkery et.al. (2011) has also used the K562 cells that were stained by the CM-Dil dye to give a red fluorescence color. These cells were then transplanted into the zebrafish embryos and the embryos were then kept for 1hr at 28°c for a recovery period and this aided in enhancing the embryos' survival rate [105]. However, in this study, the embryos have been immediately incubated at 34°c without a recovery period and this might be the reason behind the low survival rate of the injected embryos after one day post injection. Pruvot et. al (2011) has also showed a successful transplantation of the K562 cell line into the zebrafish embryos [106].

Finally, the 10mg and 15mg ponatinib loaded PLGA-PEG-PLGA NPs of the concentration 0.001mg/ml were exposed to the injected zebrafish embryos (2dpf) after half hour after the injection. The tumor cells have not been shown to be reduced clearly over the 6 days period after injection, this could be due to the long release time of Ponatinib from the PLGA-PEG-PLGA NPs.

5.1 Limitations and future directions

Possible limitation for this study includes, its most dependent on zebrafish embryos that needed proper care and training for handling and the xenograft model required even a higher level of handling as the embryos are injured. The treated groups of the zebrafish embryos with the loaded PLGA-PEG-PLGA NPs were only observed till the ethical end point of 7-dpf, thus the effect of the loaded PLGA-PEG-PLGA NPs in reducing tumor cells were only observed for a few days

despite that Ponatinib release that could happen after few days of the endpoint. For that, xenografted embryos need to be observed for a longer period of time e.g., 10-dpf. Also, the lack of FTIR< X-ray and DSC studies, the paradox of the presence of burst release at the lowest drug concentration cannot be explained. Also, deducting background fluorescence per unit area of the fluorescence images would give better quantitative measurements.

5.2 Conclusion

In summary, zebrafish is a good animal model for investigating the cardiotoxicity associated with the anti-cancer drugs such as TKIs, to determine the optimum concentration of smart nanoparticles with the least side effects and to generate xenograft model of several cancer types.

In this study, PLGA-PEG-PLGA NPs were synthesized to carry the TKIs drugs. These NPs have shown to carry Ponatinib drug (10mg and 15mg) for a long period of time, allowing for longer circulation in the zebrafish body. The toxicity of two TKIs has also been tested on this animal model revealing the optimum concentrations that would not cause cardiotoxicity in the model. The lowest concentration of Imatinib and Ponatinib (2.5μM) is the optimum concentration with the least cardiotoxicity and better survival rate. Zebrafish animal model was also used for testing the cardiotoxicity of a range of different concentrations of loaded and unloaded PLGA-PEG-PLGA NPs and the least concentrations showed to be of low toxicity and enhanced survival rate. The concentrations 0.1 and 0.05 mg/ml of the unloaded PLGA-PEG-PLGA NPs are the best in term of low cardiotoxicity and high survival rate, while 0.001mg/ml concentration of the loaded PLGA-PEG-PLGA NPs with 10 or 15mg Ponatinib has shown to be the optimum concentration among the rest of the concentrations. Lastly, these loaded NPs have been exposed to the successfully generated CML xenograft zebrafish model, however, no obvious reduce in the tumor mass was

seen indicating the slow release of Ponatinib from PLGA-PEG-PLGA NPs.

Generally, PLGA-PEG-PLGA NPs could be good candidate for CML treatment, but their cellular internalization should be enhanced. This could be achieved by coating and labeling the surface of PLGA-PEG-PLGA NPs with specific ligands that are unique to CML cells.

Chapter 6: Appendix

6.1 QU-IACUC approval

جامعة قطر
QATAR UNIVERSITY

Institutional Animal Care & Use Committee (QU-IACUC)

QATAR UNIVERSITY, PO BOX 2713, DOHA, QATAR
TEL: +974 4403-6676 **FAX:** +974 4403-3901
Email: QU.IACUC@qu.edu.qa
Assurance Registration #: IACUC-QU-2019-002
Assurance #: IACUC-A-QU-2019-0004

January 7th, 2021

TO: **Dr. Huseyin Yalcin,** Biomedical Research Center, Qatar University
Email: hyalcin@qu.edu.qa

FROM: Qatar University - Institutional Animal Care & Use Committee (QU-IACUC)

SUBJECT: **Letter of IACUC Protocol Approval (QU-IACUC 019/2020) – Designated Member Review (DMR)**
Project Title: "Development and in vivo testing of smart nanoparticles for enhanced anti-cancer activity and reduced cardiotoxicity associated with Tyrosine kinase inhibitors"

Grant: QUST-2-CHS-2020-11

Dear Dr. Huseyin,

The Qatar University Institutional Animal Care and Use Committee (QU-IACUC) has **APPROVED** by the designated member review the above referenced Animal Use Protocol **# QU-IACUC 019/2020.**

Date of Initial Approval: January 7, 2021 **Date of Expiration:** January 6, 2022

The IACUC staff will make every effort to send the Principal Investigator annual reminders. However, it is the Principal Investigator's sole responsibility to submit needed renewals and Annual Review **at least one month in advance** of the annual review due dates to ensure continuing IACUC approval. **It is very important that these deadlines are not missed**. Failure to submit an Annual Review/Renewal on time will result in all persons listed under this protocol losing access to zebrafish facility and animal ordering and may potentially result in the termination of the protocol. QU-IACUC deals with expired protocols approvals as new submissions.

Please note that to continue this research/protocol beyond the **three-year period since its start**, a new protocol submission will be required. To avoid a lapse in IACUC approval, it is essential that the completed annual renewal protocol be submitted and approved by the IACUC prior to its expiration date.

Ministry of Public Health regulations do not permit the IACUC to extend any approval periods. If a renewal protocol has not been processed and approved by the IACUC prior to its expiry, IACUC approval for the work under the above referenced protocol will expire. Should IACUC approval expire, all activities involving the care and use of animals must cease immediately. Any activities conducted under the protocol after expiration will be in direct violation of governmental regulations and institutional/IACUC policies.

It is the responsibility of the Principal Investigator to notify the IACUC of any proposed changes regarding the work described within this protocol. The Principal Investigators listed above agree that no such changes will be implemented until approved by the IACUC, except where absolutely necessary to eliminate apparent immediate hazards to person(s) and/or animal(s).

جامعة قطر
QATAR UNIVERSITY

Kindly refer to the above Animal Use Protocol number in all of your future correspondence with us pertaining to this project.

Sincerely,

Dr. Abdelali Agouni, MSc, PhD, FHEA
Chair of QU-IACUC
Qatar University
Doha, Qatar

جامعة قطر
QATAR UNIVERSITY
IACUC
Institutional Animal Care and Use Committee

copy: QU-IACUC files

REFERENCES

1. Nagai, H. and Y.H. Kim, *Cancer prevention from the perspective of global cancer burden patterns.* Journal of thoracic disease, 2017. **9**(3): p. 448.
2. Sarkar, S., et al., *Cancer development, progression, and therapy: an epigenetic overview.* International journal of molecular sciences, 2013. **14**(10): p. 21087-21113.
3. Davis, A.S., A.J. Viera, and M.D. Mead, *Leukemia: An overview for primary care.* American family physician, 2014. **89**(9): p. 731-738.
4. Hanlon, K. and M. Copland, *Chronic myeloid leukaemia.* Medicine, 2017. **45**(5): p. 287-291.
5. Winkler, G.C., et al., *Functional differentiation of cytotoxic cancer drugs and targeted cancer therapeutics.* Regulatory Toxicology and Pharmacology, 2014. **70**(1): p. 46-53.
6. O'Brien, S.G., et al., *Imatinib compared with interferon and low-dose cytarabine for newly diagnosed chronic-phase chronic myeloid leukemia.* New England Journal of Medicine, 2003. **348**(11): p. 994-1004.
7. Skubitz, K.M., *Cardiotoxicity monitoring in patients treated with tyrosine kinase inhibitors.* The oncologist, 2019. **24**(7): p. e600.
8. Hua, S., et al., *Current trends and challenges in the clinical translation of nanoparticulate nanomedicines: pathways for translational development and commercialization.* Frontiers in pharmacology, 2018. **9**: p. 790.
9. Howe, K., et al., *The zebrafish reference genome sequence and its relationship to the human genome.* Nature, 2013. **496**(7446): p. 498-503.
10. Teame, T., et al., *The use of zebrafish (Danio rerio) as biomedical models.* Animal Frontiers, 2019. **9**(3): p. 68-77.

11. Lam, S., et al., *Development and maturation of the immune system in zebrafish, Danio rerio: a gene expression profiling, in situ hybridization and immunological study.* Developmental & Comparative Immunology, 2004. **28**(1): p. 9-28.

12. Siegel, R.L., K.D. Miller, and A. Jemal, *Cancer statistics, 2019.* CA: a cancer journal for clinicians, 2019. **69**(1): p. 7-34.

13. Bray, F., et al., *Global cancer statistics 2018: GLOBOCAN estimates of incidence and mortality worldwide for 36 cancers in 185 countries.* CA: a cancer journal for clinicians, 2018. **68**(6): p. 394-424.

14. The, L., *GLOBOCAN 2018: counting the toll of cancer.* Lancet (London, England), 2018. **392**(10152): p. 985.

15. Zhang, Y., et al., *Nanotechnology in cancer diagnosis: progress, challenges and opportunities.* Journal of Hematology & Oncology, 2019. **12**(1): p. 137.

16. *QATAR NATIONAL CANCER REGISTRY - CANCER INCIDENCE - 2014*. 2016.

17. Albakr, R.B., *Incidence trend of the leukemia reported cases in the Kingdom of Saudi Arabia, observational descriptive statistic from Saudi Cancer Registry.* Clinical Lymphoma, Myeloma and Leukemia, 2015. **15**: p. S2.

18. Cokkinides, V., et al., *American cancer society: Cancer facts and figures.* Atlanta: American Cancer Society, 2005.

19. Mandanas, R.A., et al., *Role of p21 RAS in p210 bcr-abl transformation of murine myeloid cells.* 1993.

20. Raitano, A.B., et al., *The Bcr-Abl leukemia oncogene activates Jun kinase and requires Jun for transformation.* Proceedings of the National Academy of Sciences, 1995. **92**(25): p. 11746-11750.

21. Shuai, K., et al., *Constitutive activation of STAT5 by the BCR-ABL oncogene in chronic myelogenous leukemia.* Oncogene, 1996. **13**(2): p. 247-254.

22. Tinkle, S., et al., *Nanomedicines: addressing the scientific and regulatory gap.* Annals of the New York Academy of Sciences, 2014. **1313**(1): p. 35-56.

23. Wang, E.C. and A.Z. Wang, *Nanoparticles and their applications in cell and molecular biology.* Integrative biology, 2014. **6**(1): p. 9-26.

24. Kumar, N. and S. Kumbhat, *Essentials in nanoscience and nanotechnology.* 2016.

25. Jeevanandam, J., et al., *Review on nanoparticles and nanostructured materials: history, sources, toxicity and regulations.* Beilstein journal of nanotechnology, 2018. **9**(1): p. 1050-1074.

26. Hu, X., et al., *Aptamer-functionalized AuNPs for the high-sensitivity colorimetric detection of melamine in milk samples.* PloS one, 2018. **13**(8): p. e0201626.

27. Varshney, M. and Y. Li, *Interdigitated array microelectrode based impedance biosensor coupled with magnetic nanoparticle–antibody conjugates for detection of Escherichia coli O157: H7 in food samples.* Biosensors and Bioelectronics, 2007. **22**(11): p. 2408-2414.

28. Cristofanilli, M., et al., *Circulating tumor cells: a novel prognostic factor for newly diagnosed metastatic breast cancer.* Journal of clinical oncology, 2005. **23**(7): p. 1420-1430.

29. Miller, M.C., G.V. Doyle, and L.W. Terstappen, *Significance of circulating tumor cells detected by the CellSearch system in patients with metastatic breast colorectal and prostate cancer.* Journal of oncology, 2010. **2010**.

30. Wang, Z. and P.A. Cole, *Catalytic mechanisms and regulation of protein kinases*, in *Methods in enzymology*. 2014, Elsevier. p. 1-21.

31. Karnik, R., et al., *Nanomechanical control of cell rolling in two dimensions through surface patterning of receptors.* Nano letters, 2008. **8**(4): p. 1153-1158.

32. de Fougerolles, A., et al., *Interfering with disease: a progress report on siRNA-based therapeutics.* Nature reviews Drug discovery, 2007. **6**(6): p. 443-453.

33. Wagner, V., et al., *The emerging nanomedicine landscape.* Nature biotechnology, 2006. **24**(10): p. 1211-1217.

34. Wolfram, J., et al., *Safety of nanoparticles in medicine.* Current drug targets, 2015. **16**(14): p. 1671-1681.

35. Shi, J., et al., *Cancer nanomedicine: progress, challenges and opportunities.* Nature Reviews Cancer, 2017. **17**(1): p. 20.

36. Gmeiner, W.H. and S. Ghosh, *Nanotechnology for cancer treatment.* Nanotechnology reviews, 2014. **3**(2): p. 111-122.

37. Barenholz, Y.C., *Doxil®—the first FDA-approved nano-drug: lessons learned.* Journal of controlled release, 2012. **160**(2): p. 117-134.

38. Pillai, G., *Nanomedicines for cancer therapy: an update of fda approved and those under various stages of development. SOJ Pharm Pharm Sci 1 (2): 13.* Nanomedicines for Cancer Therapy: An Update of FDA Approved and Those under Various Stages of Development, 2014.

39. Mahmoudi, M., et al., *Irreversible changes in protein conformation due to interaction with superparamagnetic iron oxide nanoparticles.* Nanoscale, 2011. **3**(3): p. 1127-1138.

40. Deng, Z.J., et al., *Nanoparticle-induced unfolding of fibrinogen promotes Mac-1 receptor activation and inflammation.* Nature nanotechnology, 2011. **6**(1): p. 39-44.

41. Cho, W.-S., et al., *Progressive severe lung injury by zinc oxide nanoparticles; the role of*

Zn 2+ dissolution inside lysosomes. Particle and fibre toxicology, 2011. **8**(1): p. 1-16.

42. Molinaro, R., et al., *Polyethylenimine and chitosan carriers for the delivery of RNA interference effectors.* Expert opinion on drug delivery, 2013. **10**(12): p. 1653-1668.

43. Hamilton, R.F., et al., *Particle length-dependent titanium dioxide nanomaterials toxicity and bioactivity.* Particle and fibre toxicology, 2009. **6**(1): p. 1-11.

44. Lunov, O., et al., *Amino-functionalized polystyrene nanoparticles activate the NLRP3 inflammasome in human macrophages.* ACS nano, 2011. **5**(12): p. 9648-9657.

45. Stern, S.T., P.P. Adiseshaiah, and R.M. Crist, *Autophagy and lysosomal dysfunction as emerging mechanisms of nanomaterial toxicity.* Particle and fibre toxicology, 2012. **9**(1): p. 1-17.

46. Kedmi, R., N. Ben-Arie, and D. Peer, *The systemic toxicity of positively charged lipid nanoparticles and the role of Toll-like receptor 4 in immune activation.* Biomaterials, 2010. **31**(26): p. 6867-6875.

47. Zhou, T., C.-C. Chuang, and L. Zuo, *Molecular characterization of reactive oxygen species in myocardial ischemia-reperfusion injury.* BioMed Research International, 2015. **2015**.

48. Bostan, H.B., et al., *Cardiotoxicity of nano-particles.* Life Sciences, 2016. **165**: p. 91-99.

49. Chuang, H.-C., et al., *Cardiopulmonary toxicity of pulmonary exposure to occupationally relevant zinc oxide nanoparticles.* Nanotoxicology, 2014. **8**(6): p. 593-604.

50. Baky, N., et al., *Induction of inflammation, DNA damage and apoptosis in rat heart after oral exposure to zinc oxide nanoparticles and the cardioprotective role of α-lipoic acid and vitamin E.* Drug research, 2013. **63**(05): p. 228-236.

51. Jiménez, G., S.Y. Shvartsman, and Z.e. Paroush, *The Capicua repressor–a general sensor of RTK signaling in development and disease.* Journal of cell science, 2012. **125**(6): p.

1383-1391.

52. Regad, T., *Targeting RTK signaling pathways in cancer.* Cancers, 2015. **7**(3): p. 1758-1784.

53. Schlessinger, J., *Cell signaling by receptor tyrosine kinases.* Cell, 2000. **103**(2): p. 211-225.

54. Futreal, P.A., et al., *A census of human cancer genes.* Nature reviews cancer, 2004. **4**(3): p. 177-183.

55. Lahiry, P., et al., *Kinase mutations in human disease: interpreting genotype–phenotype relationships.* Nature Reviews Genetics, 2010. **11**(1): p. 60-74.

56. Drake, J.M., J.K. Lee, and O.N. Witte, *Clinical targeting of mutated and wild-type protein tyrosine kinases in cancer.* Molecular and cellular biology, 2014. **34**(10): p. 1722-1732.

57. Knösel, T., et al., *Tyrosine kinases in soft tissue tumors.* Der Pathologe, 2014. **35**: p. 198.

58. Nishikawa, R., et al., *A mutant epidermal growth factor receptor common in human glioma confers enhanced tumorigenicity.* Proceedings of the National Academy of Sciences, 1994. **91**(16): p. 7727-7731.

59. Paul, M.K. and A.K. Mukhopadhyay, *Tyrosine kinase - Role and significance in Cancer.* International journal of medical sciences, 2004. **1**(2): p. 101-115.

60. Deininger, M.W., et al., *BCR-ABL tyrosine kinase activity regulates the expression of multiple genes implicated in the pathogenesis of chronic myeloid leukemia.* Cancer research, 2000. **60**(7): p. 2049-2055.

61. Lenihan, D.J. and P.R. Kowey, *Overview and management of cardiac adverse events associated with tyrosine kinase inhibitors.* The oncologist, 2013. **18**(8): p. 900.

62. Lin, Y., X. Wang, and H. Jin, *EGFR-TKI resistance in NSCLC patients: mechanisms and*

strategies. American journal of cancer research, 2014. **4**(5): p. 411.

63. Schrank, Z., et al., *Current molecular-targeted therapies in NSCLC and their mechanism of resistance.* Cancers, 2018. **10**(7): p. 224.

64. Granatowicz, A., et al., *An overview and update of chronic myeloid leukemia for primary care physicians.* Korean journal of family medicine, 2015. **36**(5): p. 197.

65. Cortes, J.E., et al., *A phase 2 trial of ponatinib in Philadelphia chromosome–positive leukemias.* New England Journal of Medicine, 2013. **369**(19): p. 1783-1796.

66. Broekman, F., E. Giovannetti, and G.J. Peters, *Tyrosine kinase inhibitors: Multi-targeted or single-targeted?* World journal of clinical oncology, 2011. **2**(2): p. 80.

67. Orphanos, G.S., G.N. Ioannidis, and A.G. Ardavanis, *Cardiotoxicity induced by tyrosine kinase inhibitors.* Acta Oncologica, 2009. **48**(7): p. 964-970.

68. Hartmann, J.T., et al., *Tyrosine kinase inhibitors-a review on pharmacology, metabolism and side effects.* Current drug metabolism, 2009. **10**(5): p. 470-481.

69. Feng, B., et al., *Role of hepatic transporters in the disposition and hepatotoxicity of a HER2 tyrosine kinase inhibitor CP-724,714.* Toxicological sciences, 2009. **108**(2): p. 492-500.

70. Moslehi, J.J., *Cardiovascular toxic effects of targeted cancer therapies.* New England Journal of Medicine, 2016. **375**(15): p. 1457-1467.

71. Kerkelä, R., et al., *Cardiotoxicity of the cancer therapeutic agent imatinib mesylate.* Nature medicine, 2006. **12**(8): p. 908-916.

72. Montani, D., et al., *Pulmonary arterial hypertension in patients treated by dasatinib.* Circulation, 2012. **125**(17): p. 2128-2137.

73. Dorer, D.J., et al., *Impact of dose intensity of ponatinib on selected adverse events: multivariate analyses from a pooled population of clinical trial patients.* Leukemia

research, 2016. **48**: p. 84-91.

74. Tavares, B. and S.S. Lopes, *The importance of Zebrafish in biomedical research.* Acta medica portuguesa, 2013. **26**(5): p. 583-592.

75. Streisinger, G., et al., *Production of clones of homozygous diploid zebra fish (Brachydanio rerio).* Nature, 1981. **291**(5813): p. 293-296.

76. Spitsbergen, J.M. and M.L. Kent, *The state of the art of the zebrafish model for toxicology and toxicologic pathology research—advantages and current limitations.* Toxicologic pathology, 2003. **31**(1_suppl): p. 62-87.

77. Mizgireuv, I.V. and S.Y. Revskoy, *Transplantable tumor lines generated in clonal zebrafish.* Cancer research, 2006. **66**(6): p. 3120-3125.

78. Spitsbergen, J.M., et al., *Neoplasia in Zebrafish (Danio rerio) Treated with N-methyl-N'nitro-N-nitrosoguanidine by Three Exposure Routes at ifferent Developmental Stages.* Toxicologic pathology, 2000. **28**(5): p. 716-725.

79. Beckwith, L.G., et al., *Ethylnitrosourea induces neoplasia in zebrafish (Danio rerio).* Laboratory investigation, 2000. **80**(3): p. 379-385.

80. Berghmans, S., et al., *tp53 mutant zebrafish develop malignant peripheral nerve sheath tumors.* Proceedings of the National Academy of Sciences, 2005. **102**(2): p. 407-412.

81. Zhao, S., J. Huang, and J. Ye, *A fresh look at zebrafish from the perspective of cancer research.* Journal of Experimental & Clinical Cancer Research, 2015. **34**(1): p. 1-9.

82. Lieschke, G.J. and P.D. Currie, *Animal models of human disease: zebrafish swim into view.* Nature Reviews Genetics, 2007. **8**(5): p. 353-367.

83. Gutiérrez-Lovera, C., et al., *The potential of zebrafish as a model organism for improving the translation of genetic anticancer nanomedicines.* Genes, 2017. **8**(12): p. 349.

84. Reed, B. and M. Jennings, *Guidance on the housing and care of zebrafish danio rerio.* Guidance on the housing and care of zebrafish Danio rerio., 2011.

85. Huang, W. and C. Zhang, *Tuning the Size of Poly(lactic-co-glycolic Acid) (PLGA) Nanoparticles Fabricated by Nanoprecipitation.* Biotechnology journal, 2018. **13**(1): p. 10.1002/biot.201700203.

86. Rao, X., et al., *An improvement of the 2ˆ (–delta delta CT) method for quantitative real-time polymerase chain reaction data analysis.* Biostatistics, bioinformatics and biomathematics, 2013. **3**(3): p. 71.

87. Pucci, C., C. Martinelli, and G. Ciofani, *Innovative approaches for cancer treatment: Current perspectives and new challenges.* Ecancermedicalscience, 2019. **13**.

88. Martinelli, C., C. Pucci, and G. Ciofani, *Nanostructured carriers as innovative tools for cancer diagnosis and therapy.* APL bioengineering, 2019. **3**(1): p. 011502.

89. Albanese, A., P.S. Tang, and W.C. Chan, *The effect of nanoparticle size, shape, and surface chemistry on biological systems.* Annual review of biomedical engineering, 2012. **14**: p. 1-16.

90. Maeda, H., *Toward a full understanding of the EPR effect in primary and metastatic tumors as well as issues related to its heterogeneity.* Advanced drug delivery reviews, 2015. **91**: p. 3-6.

91. Gerlowski, L.E. and R.K. Jain, *Microvascular permeability of normal and neoplastic tissues.* Microvascular research, 1986. **31**(3): p. 288-305.

92. Wickramasinghe, C.D., et al., *Concepts in cardio-oncology: definitions, mechanisms, diagnosis and treatment strategies of cancer therapy-induced cardiotoxicity.* Future Oncology, 2016. **12**(6): p. 855-870.

93. Cassar, S., et al., *Use of Zebrafish in Drug Discovery Toxicology.* Chemical research in toxicology, 2020. **33**(1): p. 95-118.

94. Nishikimi, T., N. Maeda, and H. Matsuoka, *The role of natriuretic peptides in cardioprotection.* Cardiovascular research, 2006. **69**(2): p. 318-328.

95. Baba, M., K. Yoshida, and M. Ieda, *Clinical Applications of Natriuretic Peptides in Heart Failure and Atrial Fibrillation.* International journal of molecular sciences, 2019. **20**(11): p. 2824.

96. Singh, A.P., et al., *Ponatinib-induced cardiotoxicity: delineating the signalling mechanisms and potential rescue strategies.* Cardiovascular research, 2019. **115**(5): p. 966-977.

97. Zhu, X.-Y., et al., *Ponatinib-induced ischemic stroke in larval zebrafish for drug screening.* European Journal of Pharmacology, 2020. **889**: p. 173292.

98. Sulaiman, T.N.S., et al., *Assessment of the Effect of PLGA Co-polymers and PEG on the Formation and Characteristics of PLGA-PEG-PLGA Co-block Polymer Using Statistical Approach.* Advanced pharmaceutical bulletin, 2019. **9**(3): p. 382.

99. Inkson, B., *Scanning electron microscopy (SEM) and transmission electron microscopy (TEM) for materials characterization*, in *Materials characterization using nondestructive evaluation (NDE) methods*. 2016, Elsevier. p. 17-43.

100. Devulapally, R., et al., *Gemcitabine and antisense-microRNA co-encapsulated PLGA–PEG polymer nanoparticles for hepatocellular carcinoma therapy.* ACS applied materials & interfaces, 2016. **8**(49): p. 33412-33422.

101. Devulapally, R. and R. Paulmurugan, *Polymer nanoparticles for drug and small silencing RNA delivery to treat cancers of different phenotypes.* Wiley Interdisciplinary Reviews:

Nanomedicine and Nanobiotechnology, 2014. **6**(1): p. 40-60.

102. Wang, T.-Y., et al., *Ultrasound-guided delivery of microRNA loaded nanoparticles into cancer.* Journal of Controlled Release, 2015. **203**: p. 99-108.

103. Ku, S., et al., *The blood–brain barrier penetration and distribution of PEGylated fluorescein-doped magnetic silica nanoparticles in rat brain.* Biochemical and biophysical research communications, 2010. **394**(4): p. 871-876.

104. Paolini, M.S., et al., *Polymers for extended-release administration.* Biomedical microdevices, 2019. **21**(2): p. 1-24.

105. Corkery, D.P., G. Dellaire, and J.N. Berman, *Leukaemia xenotransplantation in zebrafish–chemotherapy response assay in vivo.* British journal of haematology, 2011. **153**(6): p. 786-789.

106. Pruvot, B., et al., *Leukemic cell xenograft in zebrafish embryo for investigating drug efficacy.* haematologica, 2011. **96**(4): p. 612-616.